Master Thesis

Laser-induced contamination on high-reflective optics

by
Paul Wagner
715818
University of Applied Science Darmstadt
DLR - German Aerospace Center
(Deutsches Zentrum für Luft- und Raumfahrt)

Supervisor:
Prof. Dr. Wolfgang Heddrich
University of Applied Science Darmstadt

Dr. Helmut Schröder
DLR - German Aerospace Center
(Deutsches Zentrum für Luft- und Raumfahrt)

February 2014

ABSTRACT

Operating high power space-based laser systems in the visible and UV range is problematic due to laser-induced contamination. Organic materials are outgassing in vacuum and deposit on irradiated optical components. To provide reliable space-based laser systems the optical components quality plays a major role. In this thesis laser-induced contamination growth on high-reflective coated optics is investigated for UV irradiation of 355nm with naphthalene as contamination material. Four different kinds of optics were investigated: three high-reflective coated optics fabricated by Electron Beam Deposition, Magnetron Sputtering and Ion Beam Sputtering technique and one anti-reflective coated optic fabricated by Electron Beam Deposition technique. The contamination test procedure was designed to perform laser-induced contamination tests on 45° high-reflective coated optics. For the first time in-situ observation of contamination induced damage was performed using a long distance microscope. Additionally the onset and evolution of deposit formation and contamination induced damage of optical samples was observed by in-situ laser-induced fluorescence and reflection monitoring. Ex-situ characterization of deposits and damage morphology was performed by differential interference contrast microscopy and fluorescence microscopy.
It was found that at a partial pressure of contamination material in the range of 10^{-5}mbar induced a drastic reduction of laser damage threshold compared to values obtained without contamination.

ACKNOWLEDGEMENTS

This Thesis is part of the ESA project "Optical components materials and process development and validation for high power space borne lasers". The objectives of the study has the intension to provide optics which are suitable to operate under long term space relevant conditions especially in the ultraviolet spectral range without or with reduced laser induced deposit formation and to understand the contamination process on an empirical basis.

It was performed at the German Aerospace Center, Institute of Technical Physics in Stuttgart, Germany.

Thanks to all co-workers and supervisors:
Wolfgang Riede[A], Helmut Schröder[A], Franz Hadinger[A], Gabriele Taube[A], Arne Potreck[A], Leif Humbert[A], Wolfgang Heddrich[B].

[A] *German Aerospace Center (Deutsches Zentrum für Luft- und Raumfahrt - DLR), Pfaffenwaldring 38-40, D-70569 Stuttgart*

[B] *University of Applied Science Darmstadt, Haardtring 100, D-64295 Darmstadt*

TABLE OF CONTENTS

GLOSSARY

Symbol	Explanation
DLR	German Aerospace Center (Deutsches Zentrum für Luft- und Raumfahrt e.V.)
ESA	European Space Agency
LIDAR	Light detection and ranging
LIC	Laser-induced contamination
LIDT	Laser-induced damage test
UV	Ultraviolet
AR	Anti-reflective coating
HR	High-reflective coating
MS	Magnetron sputtering
EBD	Electron Beam Deposition
IBS	Ion Beam Sputtering
Nd:YAG	Neodymium-doped yttrium aluminum garnet
LBO	Lithium triborate (LiB_3O_5)
SHG	Second harmonic generation
THG	Third harmonic generation
SP	Scroll pump
TMP	Turbo molecular pump
DIC	Differential interference contrast
UHV	Ultra high vacuum
CCD	Charge coupled device
EM CCD	Electron multiplying charge coupled device
ROI	Region of interest
RGA	Residual gas analyzer

Symbol	Explanation
λ	Wavelength
n	Refractive index
$r_{1,2}$	Reflection coefficient
H_P	Peak Fluence
E_p	Pulse energy
$r_{x,y}$	Beam radius ($1/e^2$)
R	Reflectivity

1. INTRODUCTION

Essential for global weather forecasts and further improvement of climate models are accurate wind profiles [3]. The ESA Atmospheric Dynamics Mission (ADM-Aeolus) addresses the lack of global wind profiles at high altitude in the Global Observing System. The Global Observing System is the connection of all weather related measurements, like air and water temperature, wind speed and pressure. The Atmospheric Laser Doppler Instrument called ALADIN, a space-based light detection and ranging (LIDAR) system, measures the speed of winds by detecting backscattered light and determining the Doppler shift. Hence the Doppler shift is a measure for the velocity. The distance of the measured layer is given by the runtime of the pulse in a LIDAR system.

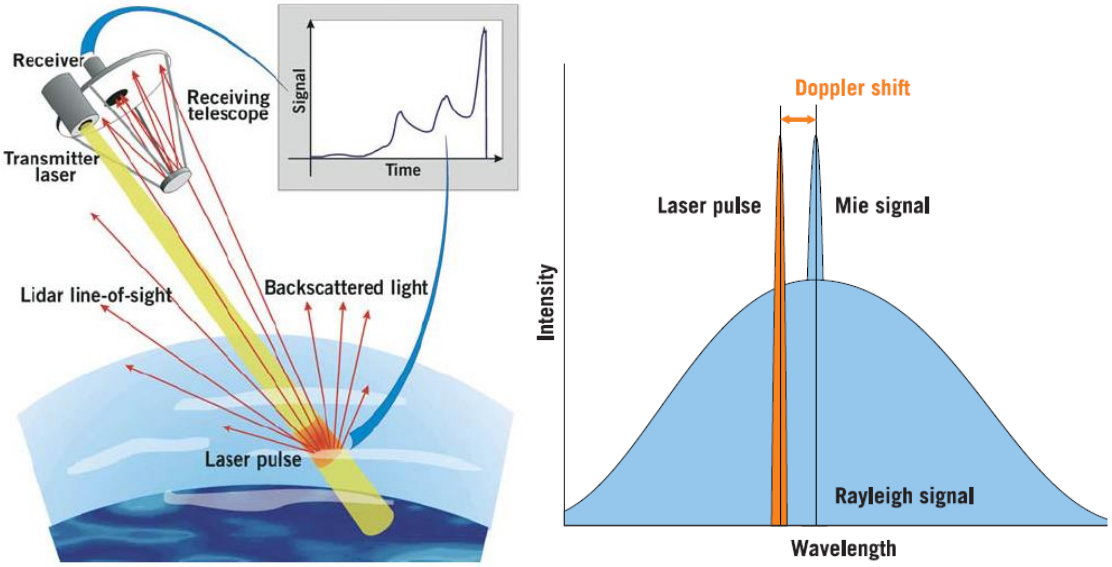

Figure 1.1: *(Left): Schematic view of a space-borne LIDAR. A short laser pulse is emitted towards the atmosphere where air molecules and particles reflect a small portion of the light pulse back to the LIDAR. A telescope collects the light and directs it to the receiver. The signal is recorded as a function of time to determine the altitude of the scattering layers. (Right): The relative motion of air leads to two effects - the center frequency of the backscattered light is shifted proportional with the wind velocity in the measurement direction, and the random motion of the air molecules leads to a broadening of the frequency width for the backscattered Rayleigh signal. Images taken from ADM-Aeolus Science Report [3].*

Critical for precise measurements is a short wavelength and high power laser. Rayleigh scattering strongly depends on the wavelength causing the higher backscattering the shorter the wavelength. A high pulse energy improves signal to noise ratio. The ALADIN instrument on board of Aeolus satellite utilizes a Nd:YAG laser frequency tripled to 355nm using nonlinear crystals.

The expected lifetime of the Aeolus satellite is 36 months with a total pulse number of 2.6×10^9. However, it has been seen that the lifetime of optics in space using visible and ultraviolet laser light is lowered due to the vacuum effect of coatings and from laser-induced contamination. Laser-induced contamination (LIC) deals with the formation of a deposit on an optical component in vacuum due to the interaction between the laser beam, the surface of the optics and outgassing organic molecules from nearby materials. To deliver reliable laser systems for long term satellite missions it is crucial to understand LIC processes.

In this thesis a closer look will be taken on the influence of laser fluence, contaminant pressure and coating structure on LIC. High reflective optical coatings are of special interest in this investigation. To determine which coating is suitable for space applications, it is investigated how contamination growth on different coatings behave and how damage occurs. Therefore contaminated conditions will be realized in an ultra-high vacuum chamber using an organic contaminant. Contamination growth and damage on optical samples will be analyzed ex- and in-situ using different instruments and methods.

1.1. INTENSION/MOTIVATION

The aim of the project is to classify optics which are suitable to be operated under long term space conditions. Since it is LIC which can shorten the lifetime of space borne laser systems operating in the UV, it is of special interest to enhance our understanding of LIC. The contamination process is not comprehended in detail and therefore it is crucial to investigate which kind of optical coating is suitable for space applications. Beside the laser-induced damage threshold (LIDT) test there is the LIC tests to investigate optic under vacuum conditions. The LIC test enforces contamination conditions under vacuum while the optical samples are irradiated with a UV laser. The laser used in the ALADIN instrument on the Aeolus satellite, has a pulsed laser with a repetition rate of 50Hz and a pulse width of 30ns. It has a wavelength of 355nm and pulse energy of 120mJ. In chapter 3 the components of the LIC test bench will be explained.

In laser systems anti- and high-reflective coatings are widely used on laser optics, and in section 2.2 the basic theoretical background of the coatings is explained. Different coating techniques are available to realize anti- and high-reflective coatings. The coating techniques are explained in chapter 2, section 2.3. Common techniques are Electron Beam Deposition (EBD), Magnetron Sputtering (MS) and Ion Beam Sputtering (IBS). EBD is the workhorse of laser optics; which allows laser optics to be used under reasonably high laser fluence under atmospheric conditions but not under vacuum. MS shows a high material quality, a high damage threshold and can be operated in vacuum. It will be shown in section 2.3 that IBS has the best known properties.

Not all coating techniques are suitable for space applications and it is of interest which coating technique shows best results in LIC tests. Anti-reflective coatings have been already tested in LIC tests with EBD and MS coated samples. Here of special interest is the examination of high-reflective coatings which have not been tested in LIC tests so far. High-reflective optics

show a higher damage threshold on LIDT than anti-reflective optics. It is of interest how high-reflective optics perform under contamination conditions in order to understand the contamination process and to be able to deliver suitable optics for space applications. The current knowledge of the contamination process will be explained in section 2.1.

All tested coatings are made by Laser Optik Garbsen GmbH on fused silica substrates and several samples of each coating technique are used which are listed in section 6.2. All samples are tested in an UHV chamber and online investigation is possible only through the chamber windows. Former tests have shown that contamination deposit shows fluorescence under UV irradiation. It is also shown in Phase I Report [1] that fluorescence correlates with deposit formation, therefore fluorescence imaging is a reliable tool to investigate the contamination growth on the optical samples. Additionally measurements of the reflectivity give a good prediction on damage occurrence on the sample. Damage formation during LIC tests was never investigated so far, so an in-situ long distance microscope is incorporated into the setup. In section 3.5 in-situ and respectively in section 3.6 ex-situ instruments used for investigations are explained.

The investigations and measurements in this thesis aim to find out how the deposit grows on the optical surface, how the damage occurs and which optical sample performs best under contaminated conditions. This allows providing optics for future space-based laser systems with a higher resistance to contamination to increase laser pulse energy and life time.

2. BACKGROUND

In section 2.1 is given a general overview on current known contamination behavior by laser-induced contamination is given.
Laser-induced contamination on several optical samples with high-reflective and anti-reflective coatings are investigated, see chapter 4. First in section 2.2 is explained how anti- and high-reflective coatings work in principle. The different coating techniques, called Electron Beam Deposition, Magnetron Sputtering and Ion beam Sputtering are described in section 2.3.

2.1. CONTAMINATION

A general problem of operating laser systems under vacuum conditions is the accumulation of organic material depositing on irradiated optical surfaces. Organic molecules are outgassing from components and materials, like glue or isolation materials (which are used in satellites). The organic molecules interact with the laser beam and form a deposition on the optic, see **Figure 2.1**. This contamination leads to a change in optical characteristics like an increased absorption and dramatic reduction of the damage threshold (up to 10 times, [16]).

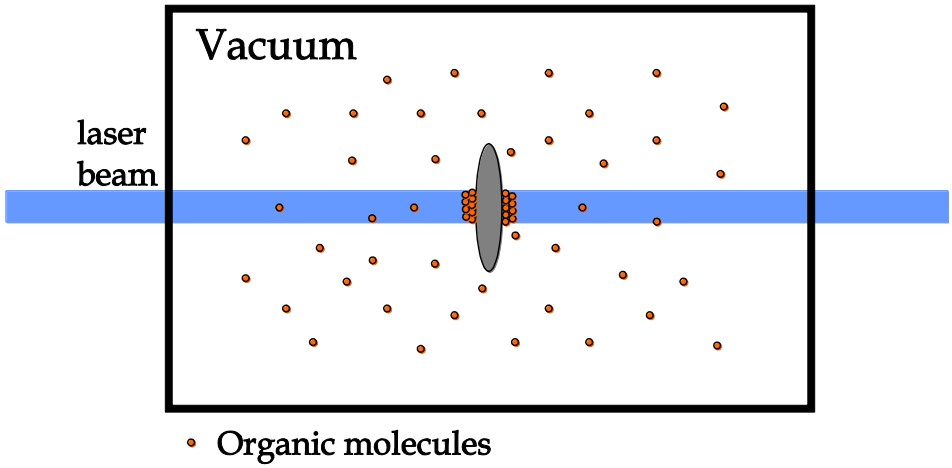

Figure 2.1: *During the contamination process in vacuum organic molecules deposit on the optical surfaces irradiated by the laser beam.*

Previous tests have shown that the contamination process depends on laser parameters (fluence, pulse frequency, wavelength), atmosphere composition (pressure, partial contaminant pressure, partial oxygen pressure) and on the coating structure of the optics [1].

To detect contamination it was seen that fluorescence correlates with deposit formation [1]. Former tests [1] have shown that optical samples with an anti-reflective coating show higher contamination than uncoated fused silica optical samples. During LIC tests with anti-reflective coating, Electron Beam Deposition (EBD) samples showed a stronger contamination than

Magnetron Sputtered (MS) samples, see **Figure 2.2**. Uncoated samples showed lower contamination compared to MS or EBD samples.

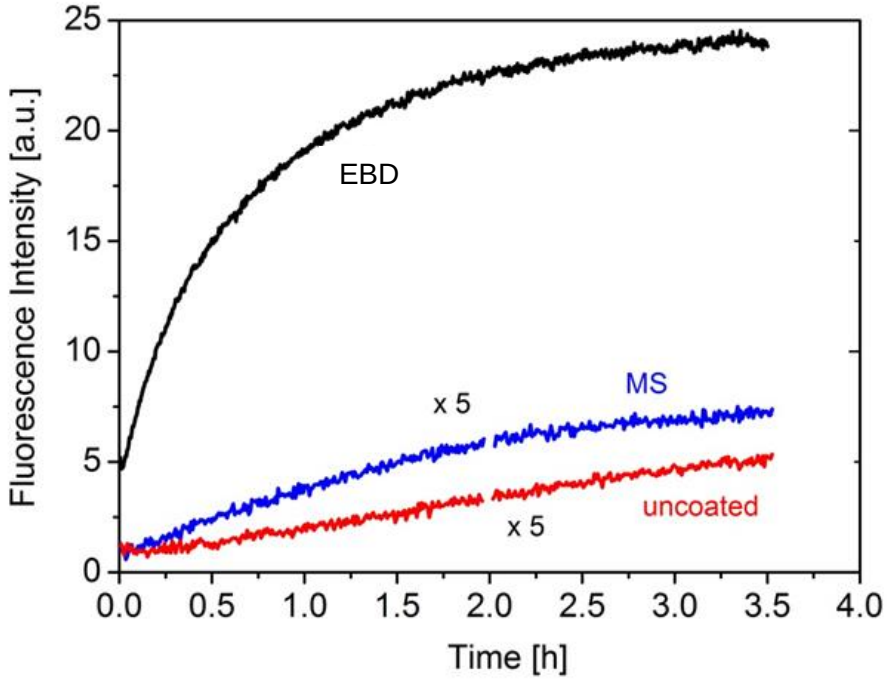

Figure 2.2: *Samples with anti-reflective coating (EBD and MS) show stronger laser induced fluorescence from the deposit, and therefore more contamination, than uncoated fused silica samples. EBD samples show more contamination then MS samples. Tested under 0° angle of incident with fluence of 7mJ/cm² and under 3.5×10^{-4} mbar naphthalene contamination pressure. AR coatings made for 355nm wavelength. Taken from Schröder et al. [16].*

Contamination growth increases with laser fluence and contamination pressure. Using same number of pulses with a lower repetition rate showed higher contamination than with a high repetition rate which implicates that growth occurs mainly between laser pulses. Deposition growth behavior on anti-reflective optics is depicted in **Figure 2.3**. Deposition starts to grow with a Gaussian shape which reproduces the laser beam profile, up to the 3rd min after irradiation started. Later ablation occurs in the center and deposition shape changes.

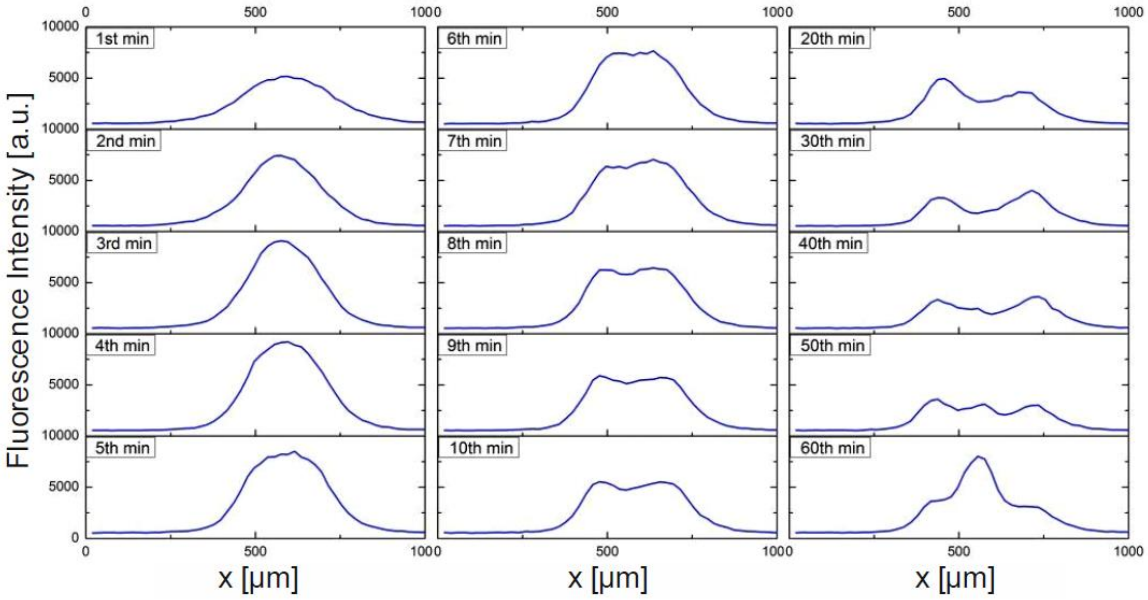

Figure 2.3: *Deposition measured by in-situ monitored laser induced fluorescence images as a function of time from top to bottom and left to right. Test conditions: EBD, 0.60 J/cm², 1000 Hz, 3.6x10⁶ pulses, 3.5x10⁻⁴ mbar Naphthalene. Figure taken from [1].*

Since LIC is due to the existence of organic molecules in the vacuum, the contamination can be prevented by using non-organic materials. Unfortunately organic materials need to be used in satellite systems and other methods need to be found to prevent contamination. Pre-conditioning (space-conditioning) can prevent further outgassing of organic molecules by heating materials above operating temperature before installation. Further solutions discussed in reference [1], in the context of contamination prevention, are the heating of critical optical components above the environmental temperature of the system or installation of suitable oxygen containing atmosphere within the cavity.

The phenomenon of contamination is still not well understood and especially the parameters governing the onset of the deposition are crucial. Another effect which drives contamination is the coating process of the optics being used. The correct choice of optical coating can reduce contamination.

2.2. OPTICAL COATING

Optical coatings are variously used in optical applications, e.g. filters, anti-reflective coatings and high-reflective coatings. They consist of nanometer thin layers which vary in refractive indices and thickness. On every interface a fraction of light is reflected and interferes with light reflected by other interfaces.

ANTI-REFLECTIVE COATINGS

To describe the principle of anti-reflective (AR) coatings the model of two ray interference on a substrate with one layer will be discussed. Basically the light waves from the two interfaces

(air-layer and layer-substrate) interfere, destructively or constructively given by their phase difference.

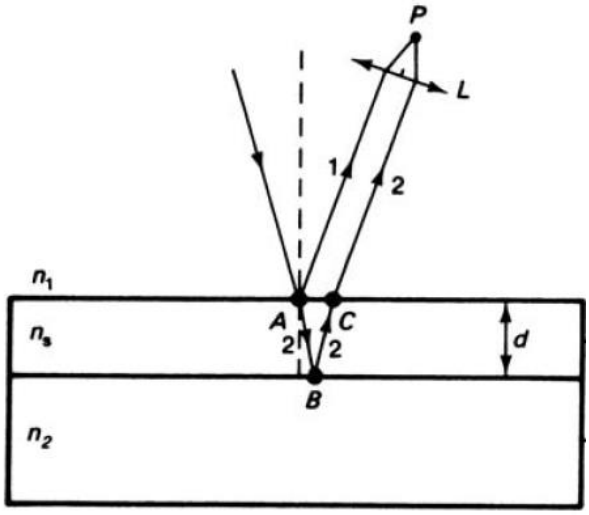

Figure 2.4: *A simple anti-reflective coating consisting of one layer can be described with two ray interference on thin layers. The ray reflected on first interface (1) interferes with the ray reflected on second interface (2). Image taken from [4].*

To realize an AR coating the destructive interference condition needs to be met. The interference is destructive if the optical path difference Δτ of two beams is an odd manifold of half the wavelength λ. Image taken from reference [4].

$$\Delta\tau = (2m+1)\frac{\lambda}{2} \qquad \text{m=0, ±1, ±2, … ,} \tag{2.1}$$

where *m* can be any integer number. The optical path difference depends on thickness *d* and refractive index n_S of the layer,

$$\tau = n_S(\lambda)\cdot d. \tag{2.2}$$

For a given wavelength λ and refractive index n_S of a material, the thickness *d* for destructive interference at an angle of incidence of 90° is given by [4],

$$\begin{aligned} \Delta\tau = (2m+1)\frac{\lambda}{2} &= n_S(\lambda)\cdot 2d \\ \mathrm{d} &= \frac{(2m+1)\cdot\lambda}{4n_S}. \end{aligned} \tag{2.3}$$

For complete cancellation the amplitude of the two interfering waves have to be the same. This means that reflected intensity needs to be same on every surface. The reflection coefficient *r* of the interface *1, 2* depends on the refractive index of surface one n_1 and refractive index of surface two n_2. For perpendicular incidence the reflection coefficient is given by [4],

$$r_{1,2} = \frac{n_1 - n_2}{n_1 + n_2}. \tag{2.4}$$

In order to achieve complete cancellation using a single layer on a substrate this results that the reflection coefficient of interface *1* and *2* need to be equal. This follows that the refractive

index of the layer n_S depend on refractive index of air n_1 and refractive index of substrate n_2 [4],

$$r_1 = r_2 = \frac{n_1 - n_S}{n_1 + n_S} = \frac{n_S - n_2}{n_S + n_2}$$
$$(n_S + n_2)(n_1 - n_S) = (n_1 + n_S)(n_S - n_2) \qquad \textbf{(2.5)}$$
$$2{n_S}^2 = 2n_1 n_2$$
$$n_s = \sqrt{n_1 n_2}.$$

Not all refractive indices can be realized since they depend on the used material and not every material can be used as it has to be scratch or chemical resistant. Using several layers allows creating broad band anti-reflective coatings and typically 3-5 layers are used in AR coatings for laser applications.

HIGH-REFLECTIVE COATINGS

The basic principle of high-reflective (HR) coatings is similar to AR coatings; instead of destructive interference condition, here the constructive interference condition of the reflected light needs to be met. Where the difference of the optical path length $\Delta\tau$ equals an even number of the wavelength [4],

$$\Delta\tau = m\lambda \qquad \text{m=0, ±1, ±2, … .} \qquad \textbf{(2.6)}$$

By using layers periodically with alternating high n_h and low refractive indices n_n the reflected light from each layer interferes constructively with light reflected from other layers.

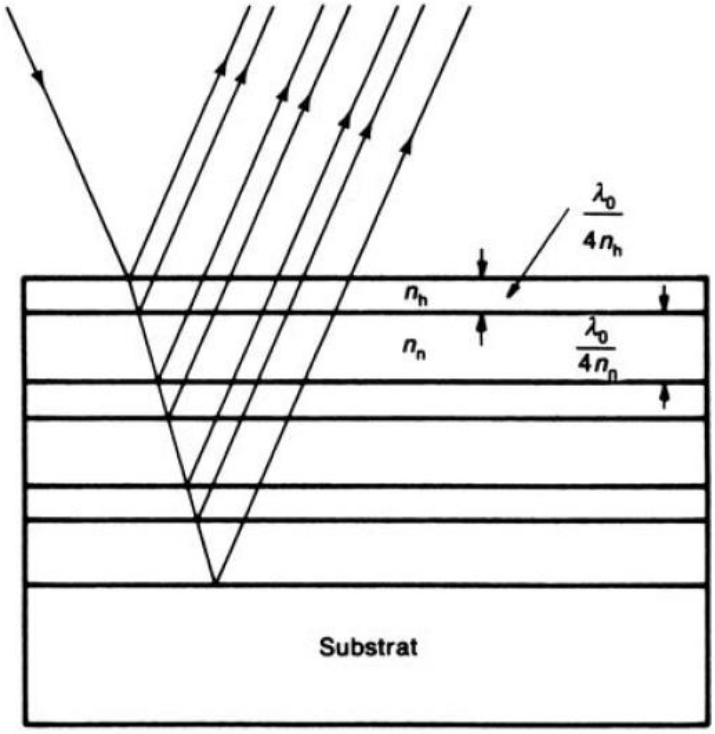

Figure 2.5: *A dielectric mirror consists of periodical layers with alternating high n_h and low refractive indices n_n. Figure taken from [4].*

A few dozens of layers are needed to realize an HR coating for a certain wavelength under a certain angle of incidence. A phase shift on interfaces with a low refractive index behind a high refractive index needs to be considered and to match constructive interference condition every layer needs an optical thickness of $\tau=\lambda/4$, [4].

2.3. COATING PROCESSES

For laser application optics are needed which withstand a high energy concentrated on a small area within a short pulse width. Therefore it is essential for laser optics to have a low absorption and high adhesive strength. The process of applying a coating on a substrate determines the coating properties like roughness, absorption or durability.

Among various techniques focus was on three different processes (Electron Beam Deposition, Magnetron Sputtering and Ion Beam Sputtering) of two methods (Evaporation and Sputtering), see **Figure 2.6**. These processes are typically used for laser optics; a thin film is realized by deposition of vaporized material (the target or coating material) on the substrate. The processes are categorized by how the evaporation is realized. In the thermal evaporation process the coating material is evaporated by an energy source. In sputter processes, instead of evaporating, the coating material is ionized and accelerated during the sputtering process. These accelerated ions are shot onto the substrate.

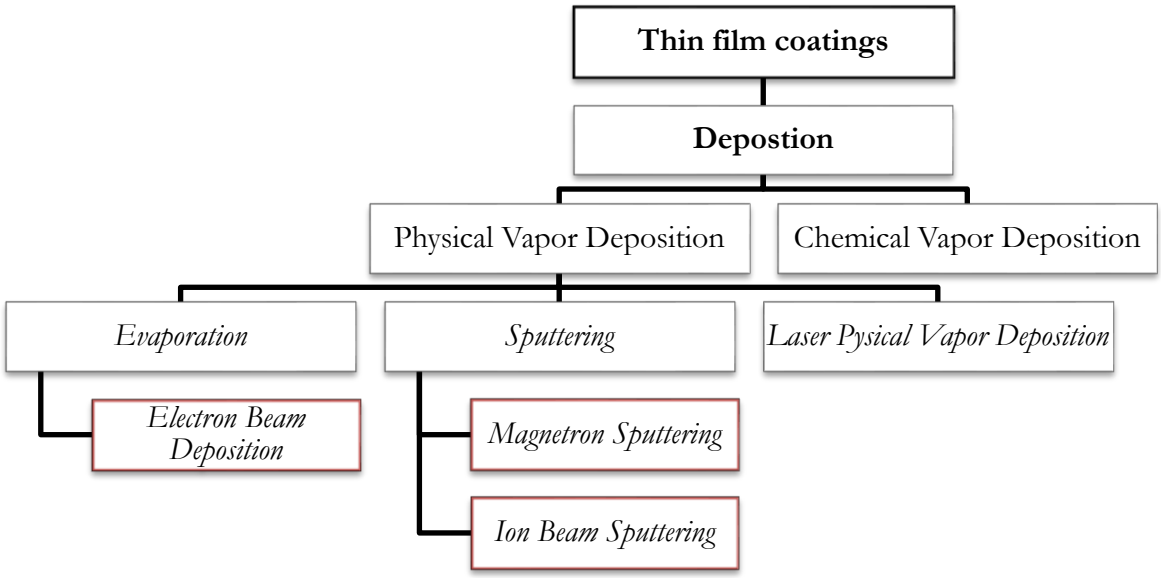

Figure 2.6: *Organogram of different techniques to produce thin films. Only those processes are shown which are of interest.*

Three different types of thin film coatings are used in LIC tests. Electron Beam Deposition is a thermal Physical Vapor Deposition process while Ion Beam Sputtering and Magnetron Sputtering are sputtering processes. Dense coatings can be produced by Sputtering techniques since density and adhesively increases with particle energy.

ELECTRON BEAM DEPOSITION

Electron Beam Deposition (EBD) is widely used for laser optics. It is one of the most common processes for producing optical coatings [10]. An electron beam heats the coating material which then evaporate, see **Figure 2.7**. These atoms have a low kinetic energy of 0.1-0.3eV.

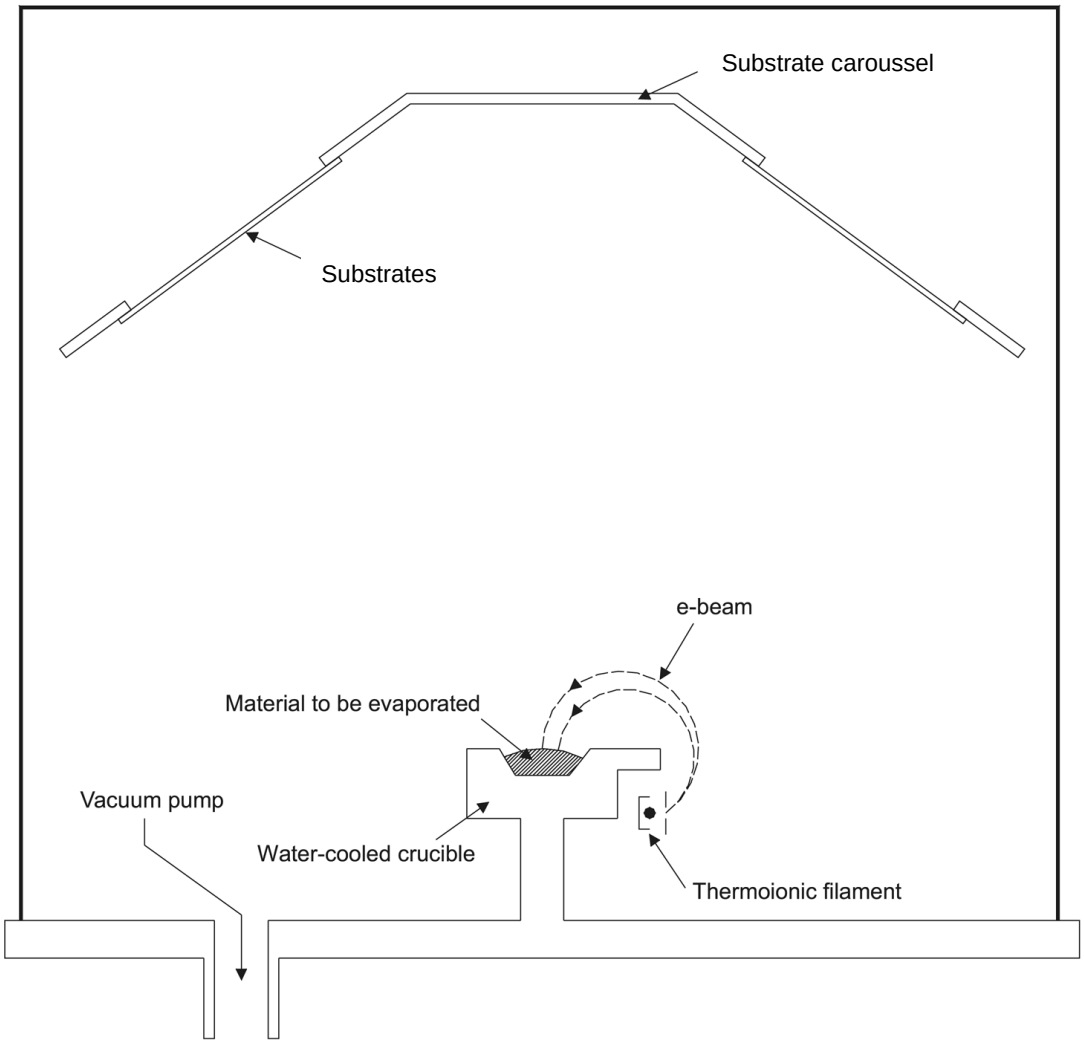

Figure 2.7: *In electron beam deposition process target material is evaporated by electron beam and deposes on substrates. The circular electron beam is due an electromagnetic field. Image taken from [6].*

During deposition on the substrate micro crystals condense in direction perpendicular to the substrate surface and form columnar structure, see **Figure 2.8**.

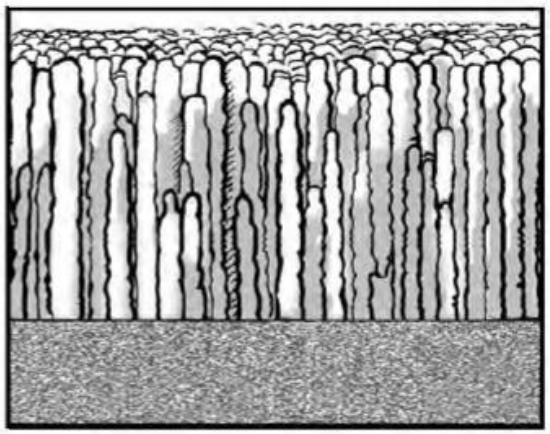

Figure 2.8: *Columnar grows of EBD coatings. Image taken from [11].*

The resulting layers are porous with a low compactness of 90%. EBD show a high laser induced damage threshold (see **Table 2.1**) which makes them suitable for laser applications. But in the porous layers of the coating gases of the atmosphere (like water) is adsorbed. Therefore EBD coatings show a so called vacuum effect, the diffusion of water and gas in and out of the layer. This mechanical stress reduces laser induced damage threshold and makes the coatings unsuitable for space applications. The coatings show a temperature drift of the reflected wavelength and high tensile stress due to water diffusing in and out of porous layers. EBD is a very effective technique which has a high reliability and allows mass production. But defect density of the coating is high with more than 100 defects per cm^{-2} [11].

MAGNETRON SPUTTERING

Using the DC-Magnetron Sputtering (MS) technique [17], [18], argon gas is ionized in a vacuum chamber by applying a voltage of several hundred volts and admitting argon gas, sees **Figure 2.9**. The ionization efficiency is increased by the magnetron. The electric field accelerates the positively charged argon ions (Ar^+) towards the cathode (the target). Here they collide with the surface of the target with a high kinetic energy of 20-100eV. The Ar^+ ions remove atoms from the surface of the metallic sputtering target. In this way, the coating material is slowly eroded. The metal atoms that are released from the target travel through the vacuum chamber. A microwave field generates oxygen plasma which reacts with the metal atoms. The oxidized metal atoms travel toward the substrate and are deposited on the substrate as a thin layer.

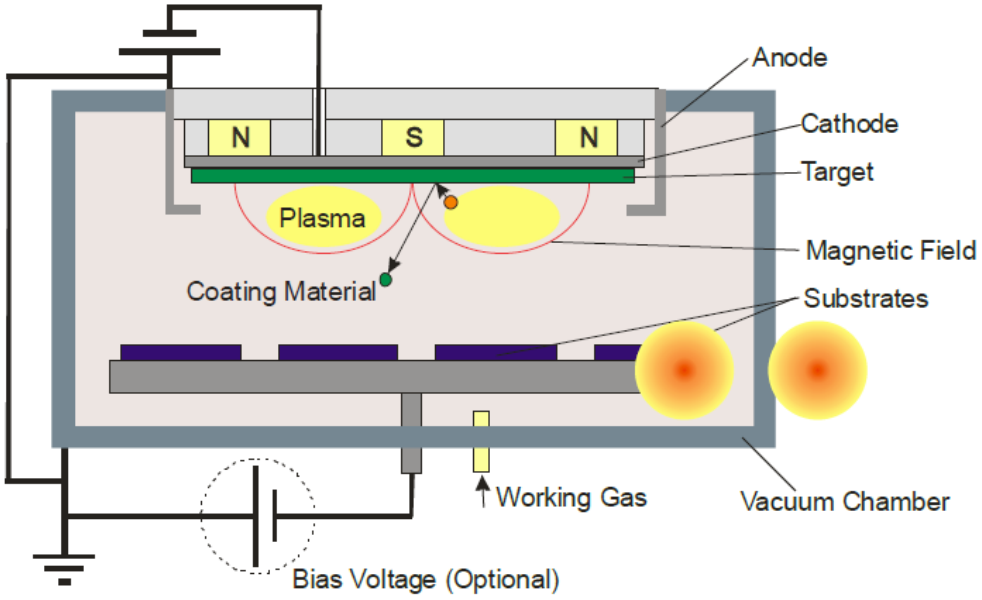

Figure 2.9: *Schematic drawing of Magnetron Sputter system. The electric field accelerates Ar^+ ions towards the target which causes the coating material to be sputtered onto the substrate. Image from [7].*

A higher kinetic particle energy of 10-20eV allows dense layers which show no vacuum effect and make these coatings suitable for space applications. Magnetron Sputtering processed coatings show a good stoichiometry between materials and have a very high laser induced damage threshold so that they are suitable for high laser power applications. Such coatings are scratch resistant but show compressive stress. This process allows faster fabrication at higher cost compared to EBD coatings.

ION BEAM SPUTTERING

Ion Beam Sputtering (IBS) utilizes an ion source to generate a focused ion beam directed at the target to be sputtered, see **Figure 2.10**. The ion source consists of a cathode and anode with a high voltage of 2-10 kV creating an electrostatic field inside the ion source. When argon gas is injected into the ion source, the high electric field causes the gas to ionize, creating plasma inside the source region. The Ar^+ ions are then accelerated from the anode region to the exit aperture (cathode) forming a collimated ion beam. The resulting ion beam impinges upon the target material and, via momentum transfer between the ion and the target atoms, sputters this material onto the sample.

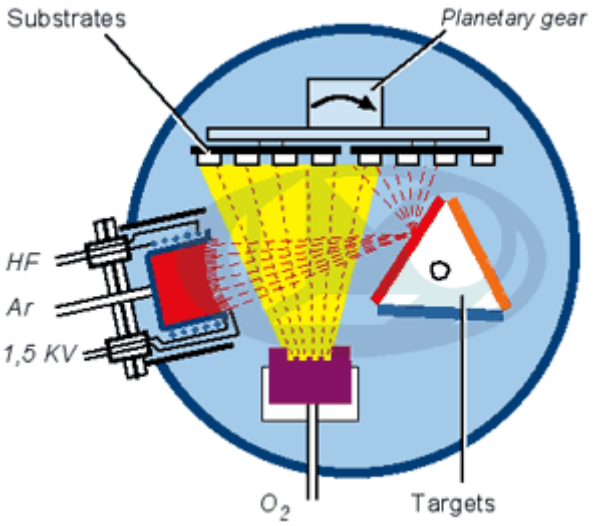

Figure 2.10: *Ion beam deposition technique accelerates ions in collimated beam onto a target. By this, material is sputtered onto the substrate. The injection of oxygen allows the target material to oxidize. Image from [11].*

A higher kinetic particle energy than EBD of 10-20eV provides a high compactness which shows no vacuum effect. Another advantage of the physical sputtering process is the lack of thermal radiation presented to the sample, allowing heat sensitive samples to be processed. This is in direct contrast to magnetron methods where samples are exposed to high energy ion bombardment and high temperatures. IBS is also a highly controllable process due to the lower deposition rates when compared with magnetron methods. This reduction in deposition rate allows for ultra-thin films to be deposited uniformly onto the sample [13].

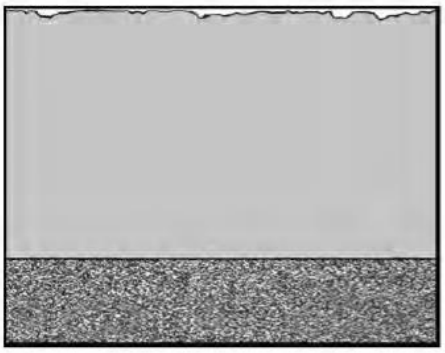

Figure 2.11: *IBS coating show very compact structure. Image taken from [11].*

Ion Beam Sputtered coatings show an excellent microstructure and high precision coatings with low defect densities of less than 1 defect per cm^{-2} [11], but internal stress. The principal drawback of IBS is the high maintenance required to keep the ion source operating [9]. Evaporation rates with IBS technique are low allowing only slow production rates with higher cost compared to MS.

CONCLUSION

In **Table 2.1** basic properties of the three different coating processes are summarized. And the investigations of samples manufactured with these coating processes are in the scope of this thesis.

	Electron beam evaporation	**Magnetron Sputtering**	**Ion Beam Sputtering**
Deposition Rate	>10 Å/sec	~10 Å/sec	~3 Å/sec
Coating area per run	1256 - 4400cm^2	> 4400cm^2	650 - 1250cm^2
Laser Damage Threshold LIDT (1064nm HR, 20ns pulse width)	~ 5 to 30 J/cm^2	~ 10 J/cm^2	>40 J/cm^2
Absorption	>100 ppm	10ppm	<2 ppm
Thermal conductivity	Low: 2x10^{-4} W/cm°C [11]	High	High: 0.09 W/cm°C [11]
Fabrication temperature range	200 - 300°C	20 - 100°C	20 - 150°C
Number of Layers	1-50	~50-100	200
Surface Micro-Roughness	+10Å RMS	<5Å RMS	<1Å RMS
Density / Porosity	Porous	Near bulk	Near bulk
Adhesion / Durability	Low	Very good	Excellent
Humidity Sensitivity	Yes	No	No
Aging Effects	Yes	No	No
Intrinsic Stress	< 100MPa	Yes, few 100MPa	Yes, few 100MPa

Table 2.1: *Comparison of different properties between EBD, MS and IBS coating processes. EBD shows lowest quality compared to the other two processes whereas IBS process shows excellent quality. Data taken from [12].*

On this basis it is expected that EBD will show worst results in LIC test with HR optics. EBD shows vacuum effect due to high porosity and compact coatings like MS and IBS have shown much better results in LIDT than EBD. On AR coatings it was found that deposit growth is much smaller on MS coatings than on EBD coatings, as seen in **Figure 2.2**. The contamination is detectable with fluorescence imaging which shows how strong the difference between MS and EBD on AR optics is, see **Figure 2.12**.

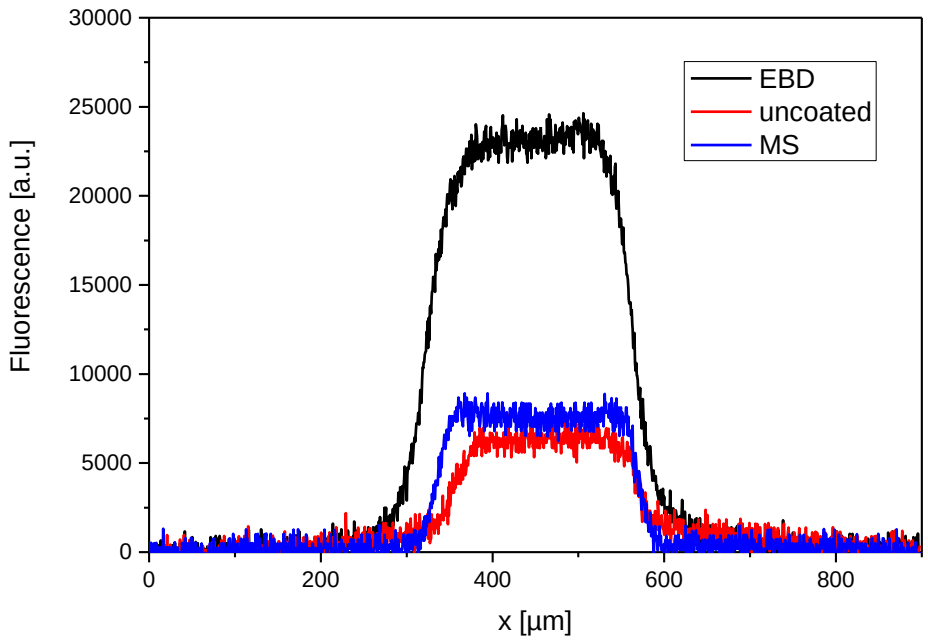

Figure 2.12: *Intensity line scans of fluorescence microscopy figures. EBD shows a higher fluorescence to MS, uncoated fused silica. Test conditions: 355 nm, peak fluence of 100mJ/cm2, 6x10^{5} pulses, naphthalene pressure of 3x10^{-4} mbar. Taken from [2].*

Anti-reflective coatings of IBS process was not tested in LIC tests but it is expected that this high quality coating will show the best results.

3. LASER-INDUCED CONTAMINATION TEST BENCH

In order to perform laser-induced contamination tests for space optics a test procedure has been developed, as there is no standard test to measure and qualify laser-induced contamination. Space conditions are replicated in the ultra-high vacuum chamber (UHV) chamber. The contamination process is enforced by specifically evaporating an organic contaminant into the UHV chamber. An UV laser with similar properties as the one operating in ALADIN is used to irradiate optical samples which are placed inside the UHV chamber. A fast repetition rate of 1000Hz and high contaminant concentration compared to laser systems working under space conditions are used during LIC tests. This allows rapidly growing contamination and better investigation of the contamination process. The existing LIC test bench [1] was modified to allow investigation of 45° HR coated optics with a special interest in in-situ damage imaging with a long distance microscope, see **Figure 3.1**.

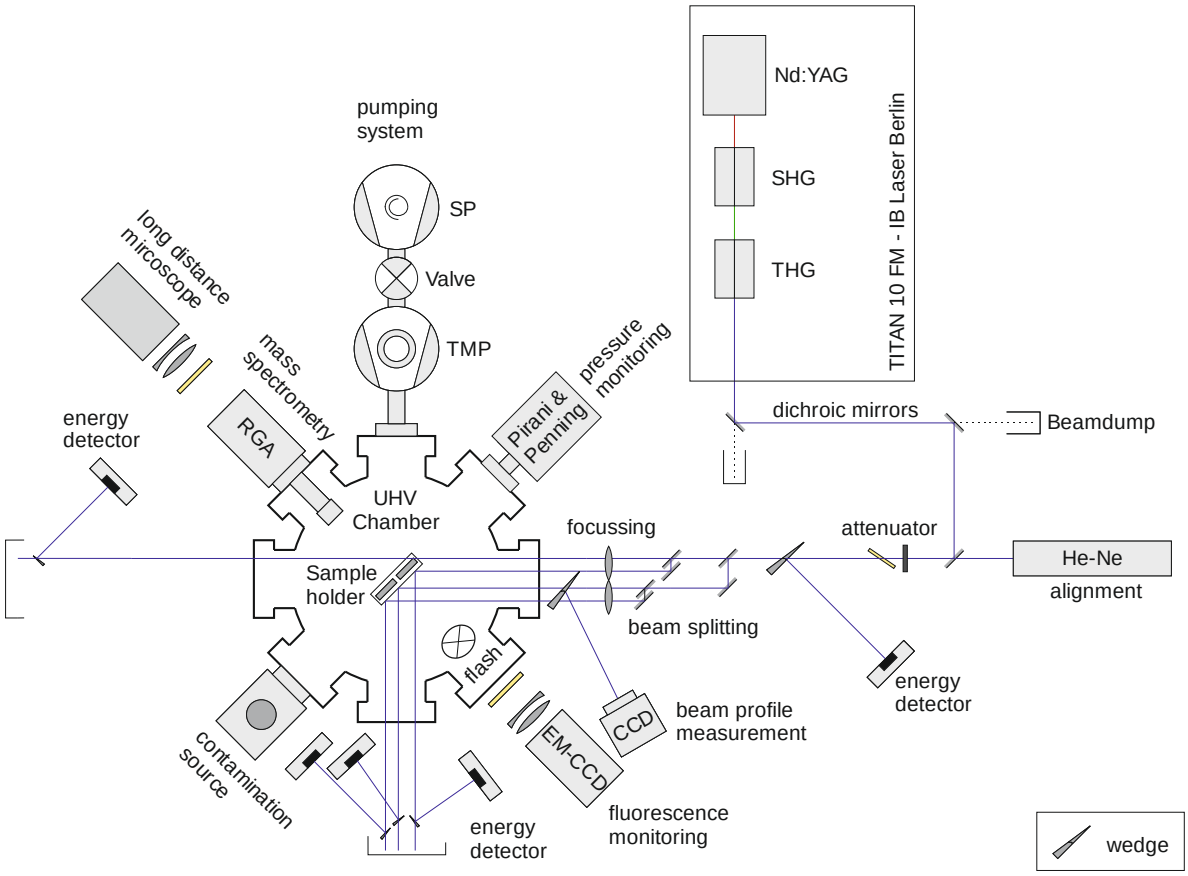

***Figure 3.1**: Laser-induced contamination test bench for testing HR coated optics.*

The setup contains three main components. The beam line with a frequency tripled Nd:YAG laser as UV laser source is described in section 3.1 and 3.2. The ultra-high vacuum chamber connected to a turbo molecular pump (TMP) and contamination source is described in section 3.3 and 3.4. The monitoring units are described in 3.5, as there are energy detectors, a mass spectrometer, a long distance microscope, laser induced fluorescence imaging and pressure monitoring. In **Figure 3.1** a schematic view of the LIC test bench is shown and in **Figure 3.2** an image of the setup taken in the laboratory is shown.

Before irradiation, the samples are cleaned using a drag & drop method with ultrapure acetone. Additional ozone cleaning is performed by placing the samples for 24h under a UV lamp which generates the ozone.

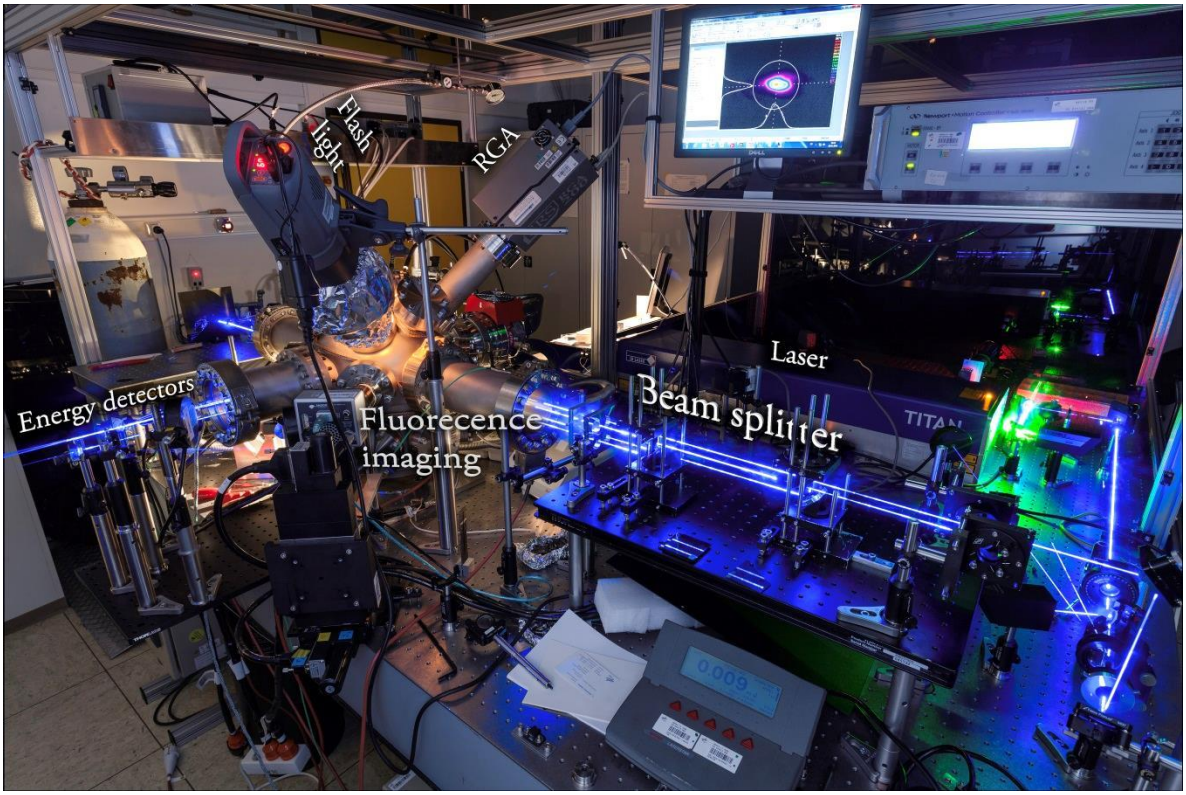

Figure 3.2: *The LIC test bench in the laboratory. From the Titan laser (far right) the UV light is split into four separate beams (front). Connected to the UHV chamber (left) is the flash light (top left), mass spectrometer (top right), the EMCCD camera for fluorescence imaging (front left) and energy detectors (left).*

The sample holder gives the possibility to host four samples with a size of 1". A translation stage gives the possibility to perform several tests on the samples under same vacuum conditions by moving samples in one plane (y – up and down). To allow irradiation of four optics simultaneously the laser beam is split into four separate beams.

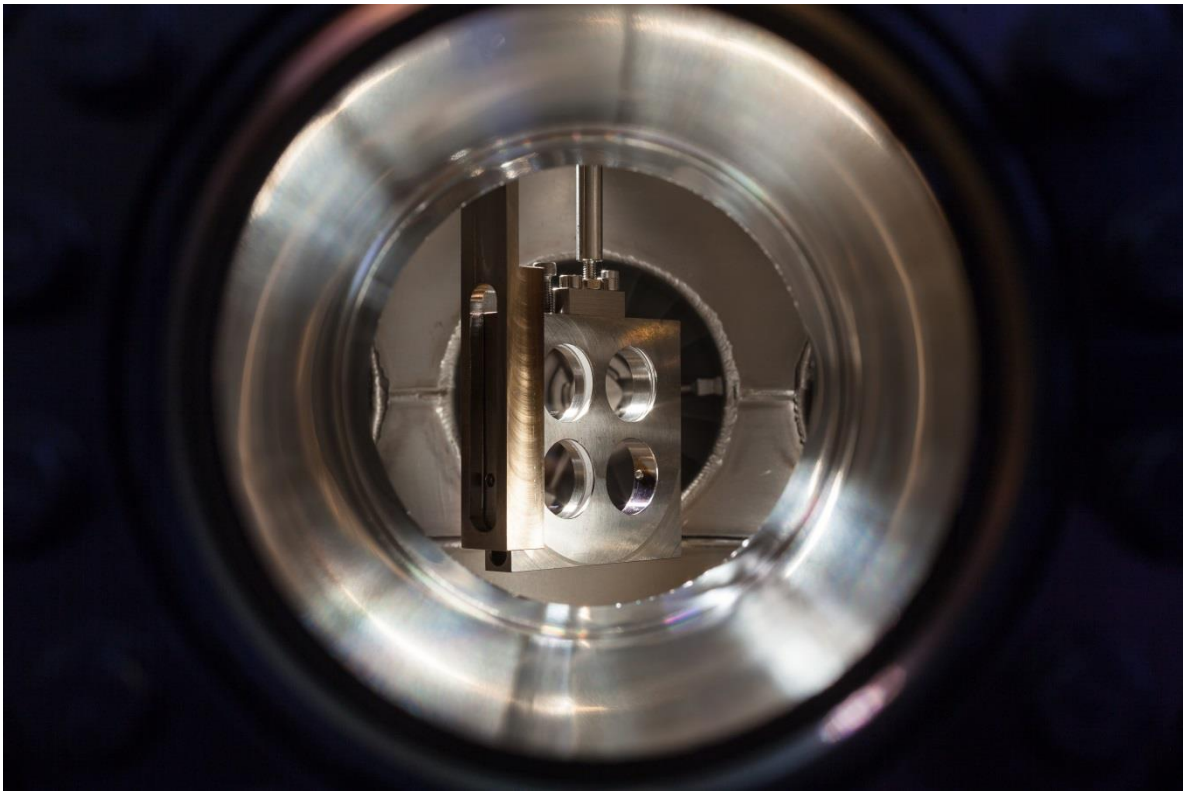

Figure 3.3: *The sample holder inside the UHV chamber during LIC test, in the back the TMP can be seen.*

To investigate tested samples after LIC test two microscopes are available. The differential interference contrast microscope allows investigation of damage morphology and the fluorescence microscopy allows high resolution contamination investigation, see section 3.6.

3.1. LASER SOURCE

The UV light is produced by a Q-switched Nd:YAG laser, which is frequency doubled via SHG and subsequently tripled via nonlinear wave mixing with two LBO (Lithium Triborate) crystals. Nanosecond pulses are achieved by frequency modulation (FM) modelocking technique. The output energy is controlled by varying the Q-switch delay time. The Titan 10FM by IB Laser has a repetition rate tunable up to 1kHz. This enables to replicate the space missions lifetime within a short time. Repetition rate of 1kHz is used in LIC tests. Pulse energy (resp. power) can be changed without major impact on the beam profile; a summary of the laser properties is given in **Table 3.1**.

Parameters	Values
Wavelength [nm]	1064, 532, 355
Pulse energy [mJ]	E_p=9.2 @1064nm
	E_p=5.2 @532nm
	E_p=1.9 @355nm
Max. repetition rate [Hz]	1000
Pulsewidth [ns] @1064nm	10
Beam quality [M^2] @1064	<1.3
Pulse-to-pulse stability @1064nm	<1%
Polarization Linear	100:1

Table 3.1: *Properties of the IB Laser Titan 10FM used for LIC tests.*

3.2. OPTICAL SETUP

Directly behind aperture of the laser dichroic mirrors (HR @355nm) are used to filter the first and second harmonics (1064nm and 532nm) of the laser light. They are absorbed by two beam dumps and only the UV laser light with a wavelength of 355nm is directed to the optical setup. A He-Ne laser is coaligned into the beam line using a HR mirror for 355nm with high-transmission for 632nm. This allows eye save alignment without affecting any samples. An optical attenuator is used to adjust laser power, consisting of a half wave plate and a thin film polarizer. An energy detector measures the energy right after the attenuator. It measures the incoming power and is used for reflection data processing explained in section 3.5. For energy detection beam is split by an optical wedge.

In order to compare several optical samples simultaneously the beam is split into four identical beams by 50/50 beam splitters. One of the four beams is used as a reference; it passes the vacuum chamber but no optical sample. Focusing lenses with a focal length of 500mm ensure that the beam diameter is larger on vacuum chamber windows than on sample surface. Consequently the energy density is considerably lower than on the optical samples. This ensures that contamination is mainly formed on the optical samples and not on the windows.

Three HR coated samples with an angle of incidence of 45° can be placed in the sample utility unit and reflect the separated laser beams. Energy of each beam is monitored after they pass the UHV chamber.

BEAM PROFILE

A characterization of each beam profile on the sample surface was measured by fitting a density profile on the spatial profile of the laser beam recorded by a CCD camera. Using software from Spiricon the waists are fitted to $1/e^2$ intensity of the beam. Those beam profiles

are taken in front of the UHV chamber. The beam is split by an optical wedge and neutral density filters are used in front of the CCD camera to prevent sensor become saturated. Below in **Figure 3.4** are the measured beam profiles at the sample plane. The beam profiles show a Gaussian beam shape but not exhibit perfect rotational symmetry.

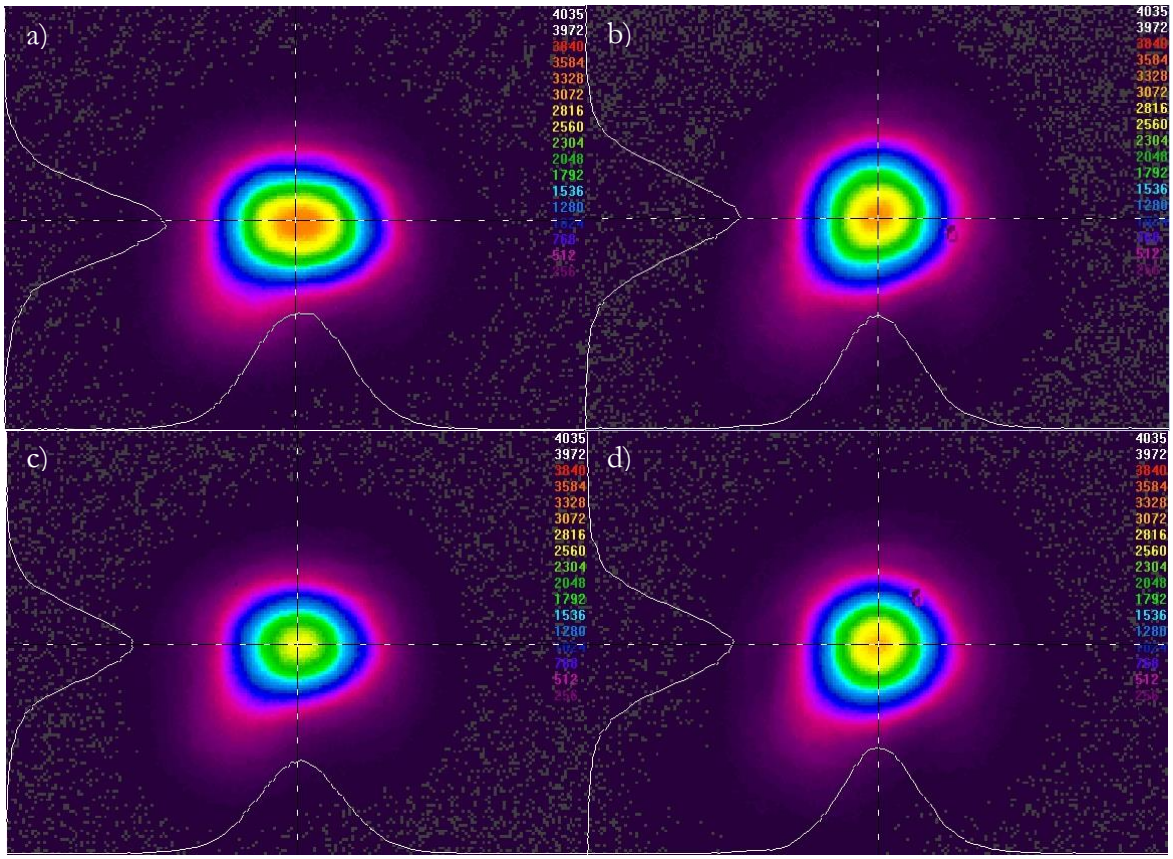

Figure 3.4: *Beam profiles at each sample position. Shown are the upper left a), upper right b), lower left c), and lower right d) sample position as seen from beam entrance port of the UHV chamber, compare* ***Figure 3.1****.*

Below in **Table 3.2** the radius in x and y direction of all four beams on each sample plane is summarized.

Sample position	Beam radius [µm]		
	r_x ±1µm	r_y ±1µm	Geometrical radius ±20µm
Upper right b)	132	132	132
Lower right d)	127	124	125
Lower left c)	136	115	125
Upper left a)	152	118	134

Table 3.2: *Beam radius on each sample position.*

The mean radius of all beams is about 130µm with a standard deviation of 9%. This allows the fluence to be below the damage threshold of samples (<5J/cm²), but high enough on samples that contamination occurs.

FLUENCE

The fluence in the laser beam profile varies; to characterize the fluence present on the sample plane the peak fluence of the Gaussian laser beam is taken.
The fluence is defined by the ratio of the pulse energy E_e and irradiated area A [4]. The peak fluence H_p is of interest because a Gaussian beam profile was measured it is calculated after equation (3.1) [19]. With a Gaussian beam shape area A is obtained by the beam radius r.

$$H_P = \frac{2 \cdot E_p}{A} = \frac{2 \cdot E_p}{\pi \cdot r_x \cdot r_y} \qquad \textbf{(3.1)}$$

The HR coated samples are tested under angle of incidence of 45°. Hence the peak fluence needs a geometrical correction because the radius in x direction becomes larger by the cos(45°).

$$H_{P\,45°} = \frac{2 \cdot E_p}{\pi \cdot r_{x\,45°} \cdot r_y} = \frac{2 \cdot E_p}{\pi \cdot \frac{r_x}{\cos(45°)} \cdot r_y} \qquad \textbf{(3.2)}$$

Any fluence using HR samples is obtained by this calculation.

The pulse energy is measured with photodiode energy detectors before beams enter the UHV chamber. In **Table 3.3** example pulse energy with corresponding fluence is shown. The peak fluence was calculated using equation (3.2) and the radius measured as previously seen in **Table 3.2**.

Sample position	**Pulse energy [mJ] ±2µJ (Q-switch: 140µs)**	**Peak fluence [mJ/cm²] ±5mJ/cm² (45°)**
Upper right b)	0.120	308
Lower right d)	0.144	409
Lower left c)	0.122	350
Upper left a)	0.117	291

Table 3.3: *Pulse energy and fluence on each sample position, testing HR optics under 45°.*

Due to variations in the beam radius and pulse energy of each beam the peak fluence varies at sample position with a standard deviation of 15% between positions. To ensure consistency of test results the samples are tested several times at different positions. The lower right position shows highest deviation from mean fluence with 20% Therefore it is used as reference beam and no sample will be placed at this position. If the fluence is stated just once for all three samples then the mean fluence at all three samples is given with a standard deviation of 15%. With a pulse energy of each beam tuneable with the attenuator from about E=0.1mJ to E=0.5mJ the fluence can be adjusted from about H_P=250mJ/cm² to H_P=1250mJ/cm².

3.3. VACUUM SYSTEM

In order to ensure reproducibility it is essential to realize stable test conditions. The laser properties are very stable over time. The vacuum system consists of commercial UHV components using CF flanges with copper sealings and is suitable for contamination tests. An UHV chamber was specifically developed for the LIC test procedure, see **Figure 3.5**. There are 21 flanges available which allow connection of turbo pump, pressure sensing, sample holder, contamination source, beam windows and in-situ measurements.

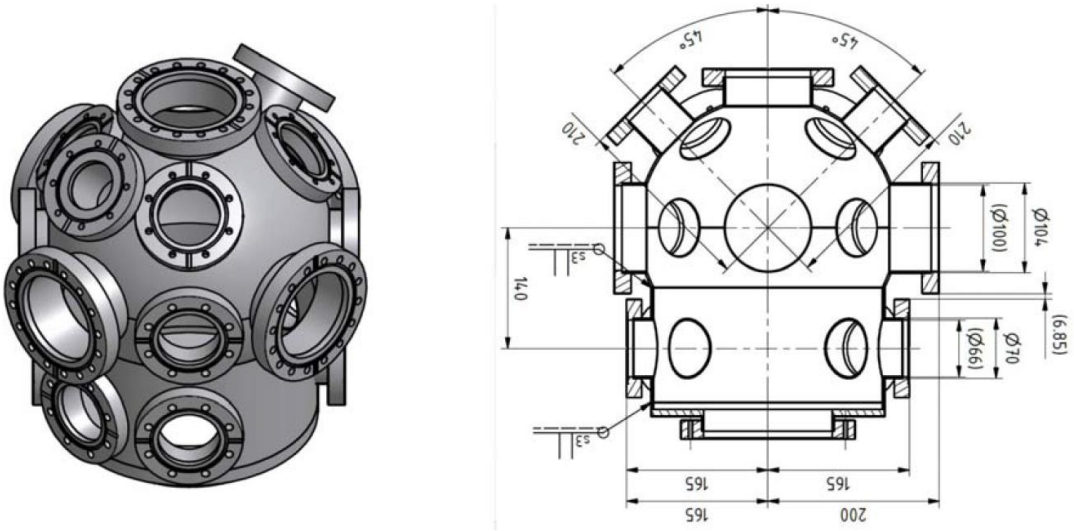

Figure 3.5: *3D sketch (left) and technical drawing (right) of the DLR developed UHV chamber for LIC tests.*

It has a diameter of about 330mm with a volume of 28.4l. Beam entrance and exit windows are coated with AR coatings for a wavelength at 355nm. These windows are connected to an extension tube in order to decrease the possibility for contaminant particles to reach and deposit on the windows, see **Figure 3.2**. Furthermore, the windows are heated at 150°C during LIC tests to prevent contamination. From previous studies it is known that thereby the contamination growth on the windows can be reduced [5].

One flange of the UHV chamber is connected by a valve to a gas bottle which allows purging the chamber with oxygen or nitrogen to perform tests under different atmospheres. The sample holder is connected to the top flange with a linear translation stage that can move the samples up and down. This allows several LIC tests of up to three different samples under same vacuum conditions.

VACUUM PUMP

To provide the vacuum a turbomolecular pump (TMP) by Pfeiffer vacuum (HiPace 300) is connected to the UHV chamber. As forepump an oil free dry scroll pump (SP) from Leybold is used. Both do not contaminate the chamber with any organic materials. A coal filter is applied to the forepump to filter contaminant.

The turbo molecular pump spins up to 1000Hz and can evacuate the chamber down to $5x10^{-9}$mbar within a couple of days. Before LIC tests the UHV chamber is evacuated for 24h.

PRESSURE SENSING

For pressure sensing two different types of gauges are used to monitor the pressure inside the UHV chamber and contamination cell during LIC tests. The Pirani gauge enables to measure a pressure in the range from 1000 to 10^{-3} mbar, while a cold-cathode type Penning gauge is sensitive in a range from 10^{-2} mbar down to $5x10^{-9}$ mbar.

3.4. CONTAMINATION SOURCE

As contamination source naphthalene, produced by Merck, was chosen because it has a high vapor pressure. This allows adjusting partial pressure accurately and this gives the possibility to remove the contaminant easily from the vacuum chamber after heating the UHV chamber for a day. Naphthalene is a crystalline powder which is transparent for 355 nm wavelength and energy of single photon is too low to ionize naphthalene.

Feature	**Value**
Formula	$C_{10}H_8$ 
Molar mass	128.17 g/mol
Ignition temperature	540°C
Solubility	0.03 g/l (25°C)
Density	1.15 g/cm3 (20°C)
Bulk density	550-600 g/cm3
Melting point	80.26°C
Boiling point	218°C
Vapor pressure	0.08 hPa (20°C)
Flash point	80°C

Table 3.4: *Properties of naphthalene. Data taken from [1].*

To ensure a constant flow of the contaminant, naphthalene is heated in the contamination chamber. The contamination chamber is a small vacuum chamber which is connected via an adjustable valve to the UHV chamber. The valve allows a constant flow of naphthalene and adjusting the partial contaminant pressure in the UHV chamber. The contamination chamber is heated to 40°C during LIC tests with typical pressure of about $6x10^{-1}$mbar. To allow a contamination pressure from $1x10^{-6}$mbar to $2x10^{-4}$mbar in the UHV chamber during LIC tests the TMP operates at 200Hz.

3.5. IN-SITU MONITORING UNITS

Several instruments are used during LIC tests for monitoring and data acquisition, which are discussed in the following sections. In order to determine the reflectivity of a HR sample, the ratio of the reflected to the incident light is measured. A decrease of 1% shows the onset of contamination and a decrease below 98% it is due to caused damage. As a function of time the reflectivity and the fluorescence, which is proportional to the contamination, is measured of each sample. Typical experimental pressures are 10^{-5}mbar and organic materials are dispensed from a source onto the samples. Hence the composition is determined of the residual gas with a mass spectrometer. With a long distance microscope images are taken in the visible range to investigate the morphology.
The laser-induced fluorescence is a good method to investigate contamination growth during LIC tests because the deposit shows fluorescence induced by the UV laser. To record contamination concentration in the UHV chamber a mass spectrometer is used. For damage growth investigations a long distance microscope takes images of the sample surface through a window of the UHV chamber.

REFLECTION

Five calibrated photo diode energy detectors (Ophir, PD10-v2) are used to measure the pulse energy. A small proportion of the beam is reflected by the optical wedge which is proportional to the input energy at the sample. Online energy monitoring of the beam is performed after every of the four beams passed the UHV chamber. One of the four beams is for reference and does not irradiate a sample, see **Figure 3.6**.

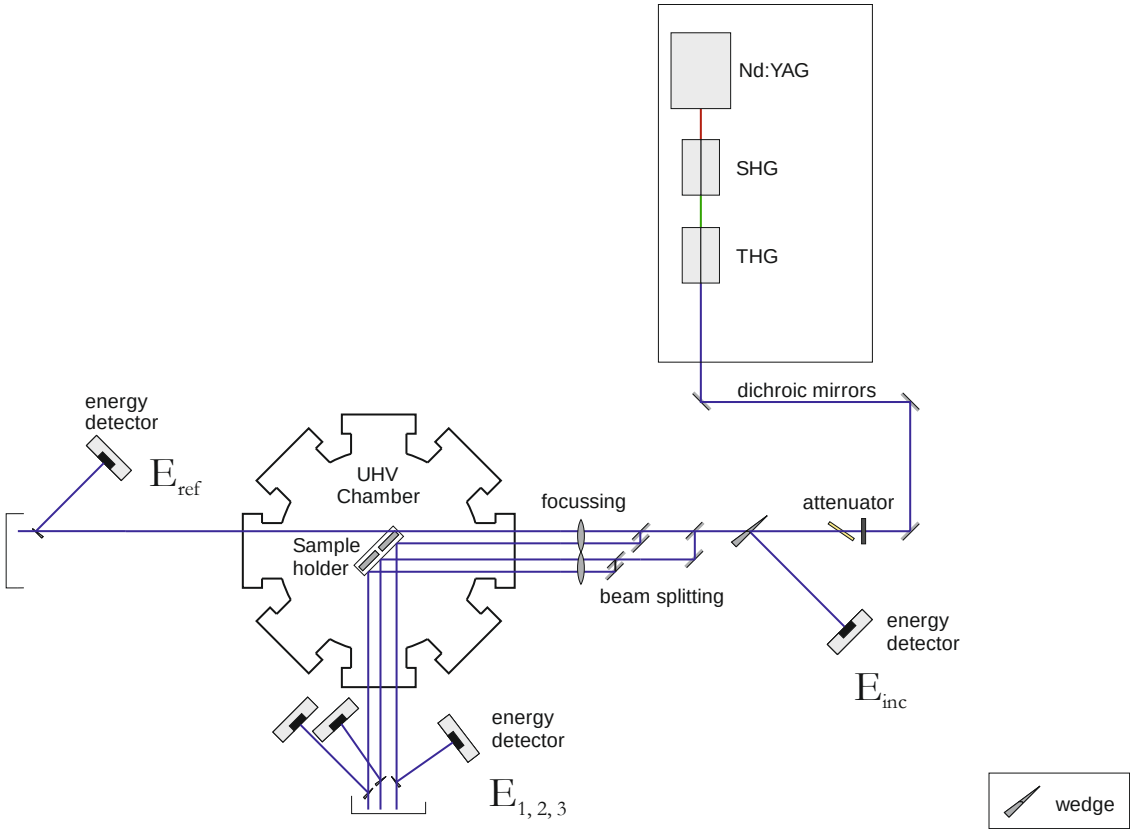

Figure 3.6: *Energy detectors recording the pulse energy of the incident beam E_{inc}, the reference beam E_{ref} and the sample beams $E_{1,2,3}$.*

To process the energy data each of the four signals $E_{1,2,3,ref}$ are divided by the incoming beam signal E_{inc}.

$$R_{1,2,3,ref} = \frac{E_{1,2,3,ref}}{E_{inc}} \tag{3.3}$$

Afterwards the signals are normalized to peak reflectivity. After normalization the reference signal which passes the UHV chamber is subtracted from every sample signal to remove the influence of chamber windows with the beam.

$$R_{1,2,3\ norm\ corr} = \frac{R_{1,2,3}}{max(R_{1,2,3})} - \frac{R_{ref}}{max(R_{ref})} \tag{3.4}$$

This gives the corrected normalized reflection R of each sample channel, 1, 2, 3.

LASER-INDUCED FLUORESCENCE IMAGING

The intensity of the fluorescence is proportional to the thickness of the deposited material hence used to investigate the growth of the contamination [1]. The organic deposition is fluorescing on UV irradiation by the laser which allows to record fluorescence with a sensitive camera. An electron multiplier CCD (EM CCD) camera from Andor (Luca) is used to detect even a small amount of the light emitted from the surface of a sample. EMCCD cameras are highly sensitive and are able to detect single photons. Connected to the camera is a microscope zoom lens with a tunable magnification from 0.7 to 5. UV light from the laser is blocked with a

filter transmissive for wavelength between 450nm-1030nm. A motorized translation stage by Newport moves the EMCCD camera and lens to record all three samples consecutively with an exposure time of 10ms. An image of every sample is recorded twice a minute.

For analysis a region of interest (ROI) with constant dimension was defined for every sample in the fluorescence image. From this region fluorescence intensity is obtained. In **Figure 3.7** are examples of images taken during the test and analyzed with the software by Andor.

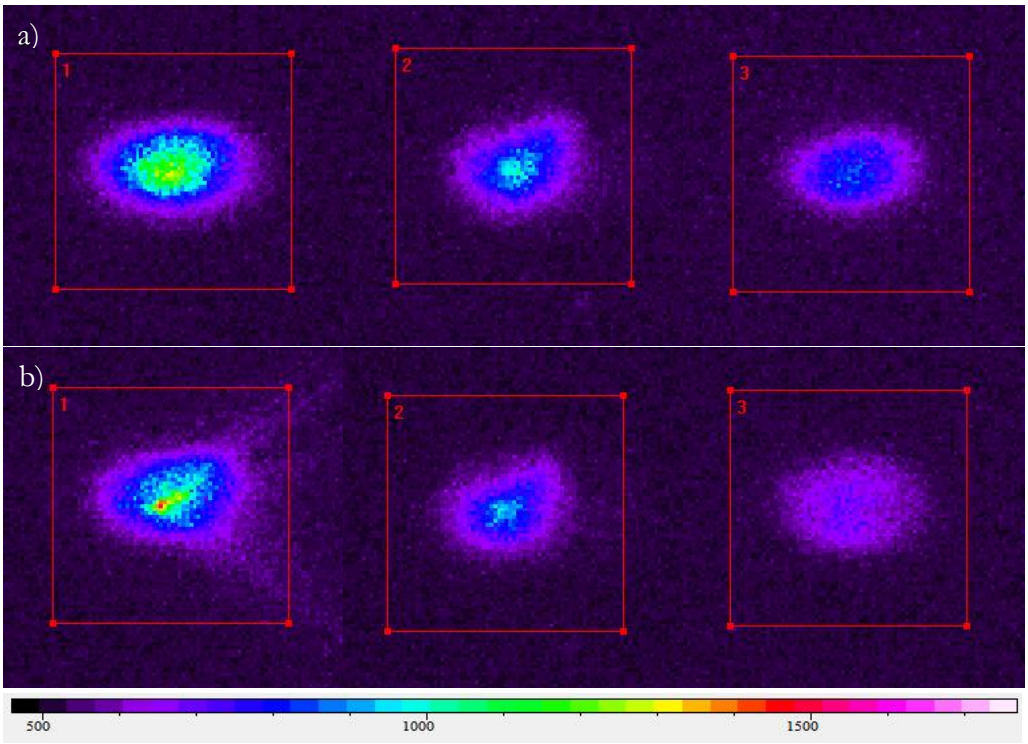

Figure 3.7: *Example images of laser-induced fluorescence recorded during LIC test. From left to right samples coated with IBS (1), MS (2) and EBD (3). First row a) shows fluorescence after 5min and second row b) after 30min. ROI is displayed in red.*

MASS SPECTROMETER

For LIC investigations it is crucial to know that the composition of the residual atmosphere present in the UHV chamber is contaminant. Therefore a residual gas analyzer (RGA) with quadrupole mass spectrometer is used to determine the atmospheric composition in the UHV chamber. The RGA uses a standard Faraday cup detector and has a maximum operating pressure of 10^{-4}mbar. Electron multipliers cannot be used due to maximum operational pressure of 10^{-6}mbar. The RGA is capable to test the mass range between 1amu and 200amu with resolution better than 0.5amu at 10% peak high, with a detection limit at a partial pressure of $5x10^{-11}$mbar.

By plotting the partial pressure over the mass certain fractions of naphthalene can be identified and in **Figure 3.8** a sample mass spectrum of the contaminated UHV chamber is shown. Naphthalene shows fragmentation peaks in the mass spectrum at several lower masses than the molecular ion peak, generated by the electron ionization mass spectrometry. Remains of air

compounds (N_2, O_2) can be seen by the molecular ion peaks but mainly naphthalene is present in UHV chamber.

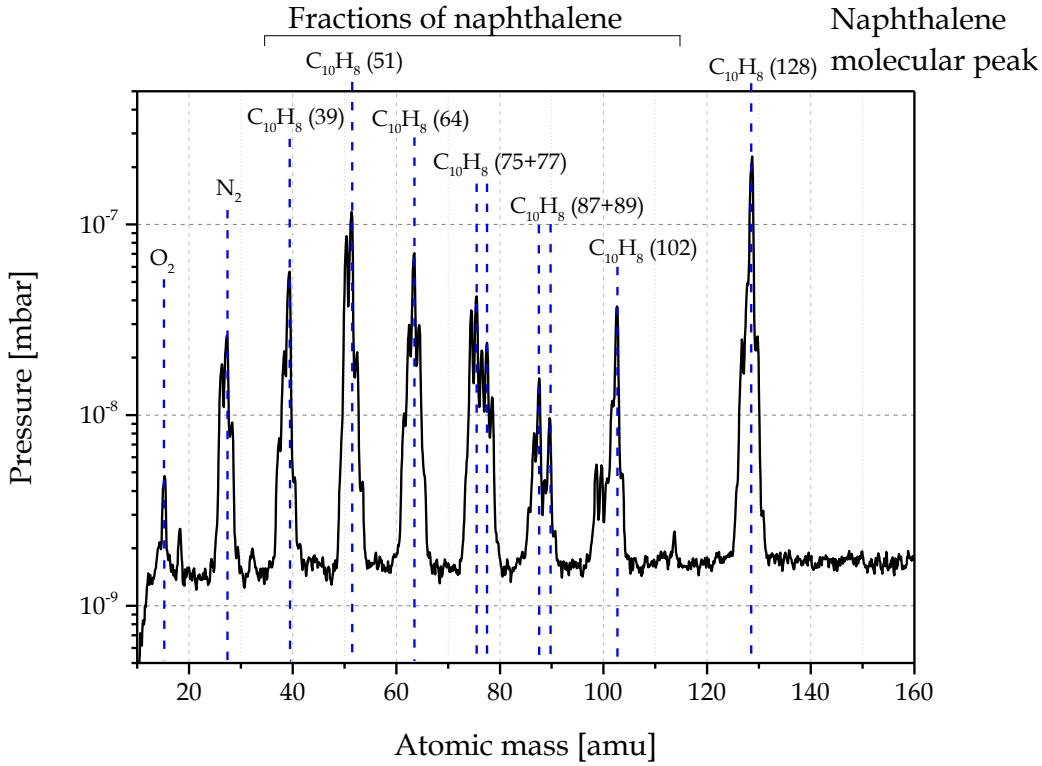

Figure 3.8: *A sample mass spectrograph which is typical for a contamination pressure of 3.5x10^{-5} mbar recorded by the RGA.*

It can also be used to identify variations of residual gas that occur during tests by tracking the partial pressures of selected masses. Tracking over time of three different fragments of naphthalene (128amu, 64amu and 51amu) in the UHV chamber for a duration of 12h 30min is shown in **Figure 3.9**.

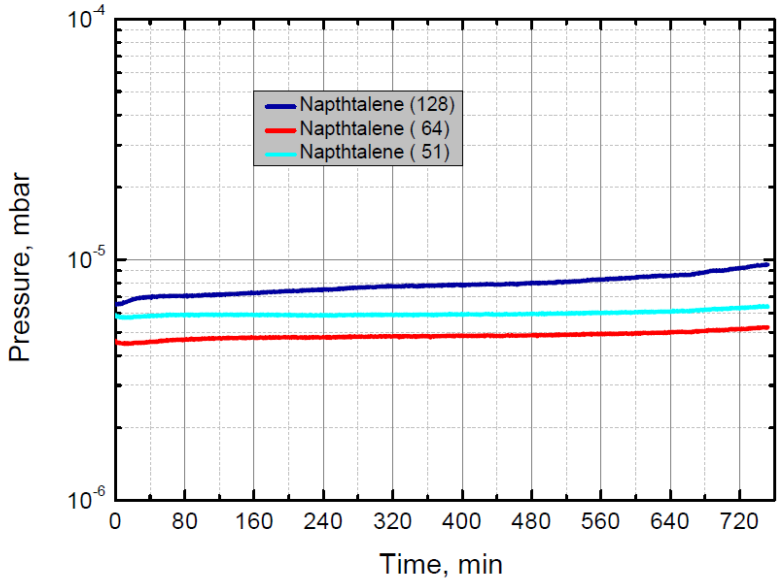

Figure 3.9: *Tracking partial naphthalene pressure over 750min in the UHV chamber. Graph taken from [1].*

An average contamination pressure of every LIC test will be stated but the pressure of naphthalene rises by 30% within 12.5h. Therefore the average contamination pressure is fluctuating in short tests (<2h) about 10%, on longer test runs 2-8h about 20% and on long time runs (>8h) about 30%.

LONG DISTANCE MICROSCOPE

To investigate the damage morphology in detail a long distance microscope QM 100 was used. It takes images of one sample during LIC test and allows to record the contamination induced damage.

It consists of a Maksutov-Cassegrain Catadioptric lens design made by Questar. The QM 100 is a microscope allows resolving structures of 10µm through a UHV chamber window in a distance of 200mm. To block the UV light from the laser a low pass filter is placed in front of the camera sensor filtering wavelengths below 420nm.

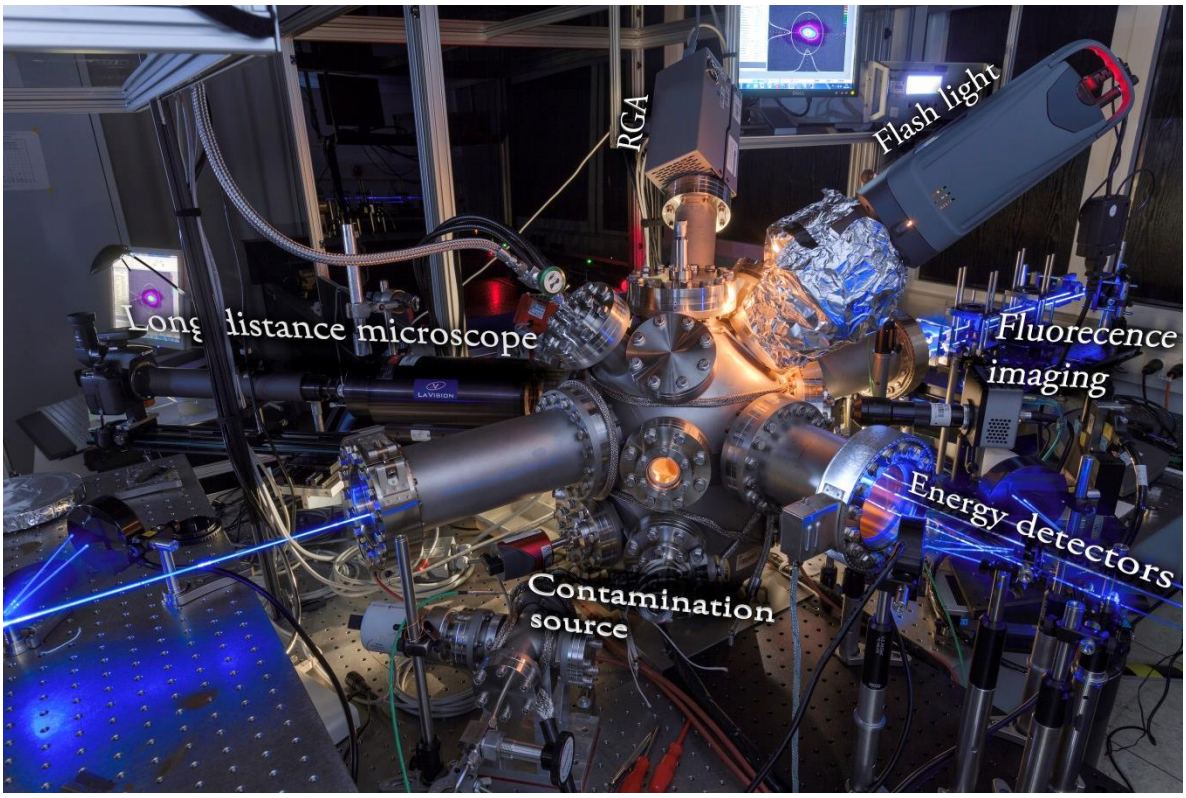

Figure 3.10: *The long distance microscope (left from the chamber) and flash light (top right from the chamber) for taking images of samples with a high magnification and contrast during LIC tests. At the bottom of the UHV chamber is the contamination source (bottom, center). The pulse energy of the reference beam (left) and probe beams (right) are detected with energy detectors.*

The large illuminated area of the microscope allows using a large sensor which gives a large field of view for better alignment of the long distance microscope. As camera a single lens reflex camera (Canon 450D) was chosen. It gives the possibility to trigger a flashlight and the camera software allows capturing images remotely at a given interval. The camera uses a CMOS sensor with a Bayer filter for color imaging. The optical resolution of the microscope is

limited by the UHV chamber window because it is positioned right in front of the microscope. A ray displacement is added on off-axis rays which cause aberrations. The image gets blurred which cannot be corrected by focusing. That is why the sensor resolution is higher than the optical resolution.

For high contrast imaging an external light source is needed to deliver reproducible and sufficient illumination. A highly stable flashlight is used to illuminate the samples on the front side through a chamber window. The studio flashlight Wallimex Pro VE-200 was triggered by the camera by connecting a remote trigger to the camera hot shoe. The microscope used to investigate the sample from the back side is focused on the HR coated front side. An exposure time of 10ms is sufficient to get high contrast images. A shutter frequency of 4Hz was usually used. A part of the image, taken by the camera, is cropped with a size of 1024px x 1024px which covers a field of view of about 500µm x 500µm. Contrast and color of images are enhanced to increase visibility.

3.6. EX-SITU INVESTIGATION

After LIC tests samples are examined with two different microscopy techniques. The differential interference contrast microscopy is used to examine damages occurred after LIC test and fluorescence microscopy allows more precise deposit measurements than in-situ fluorescence imaging.

DIFFERENTIAL INTERFERENCE CONTRAST MICROSCOPY

Differential interference contrast (DIC) microscopy also known as Nomarski microscopy is a method to visualize differences in optical path lengths. This allows the investigation of transparent samples like coatings. The basic principle is that linear polarized light is separated into two perpendicular polarizations taking different path through the optics which is depicted in **Figure 3.11**.

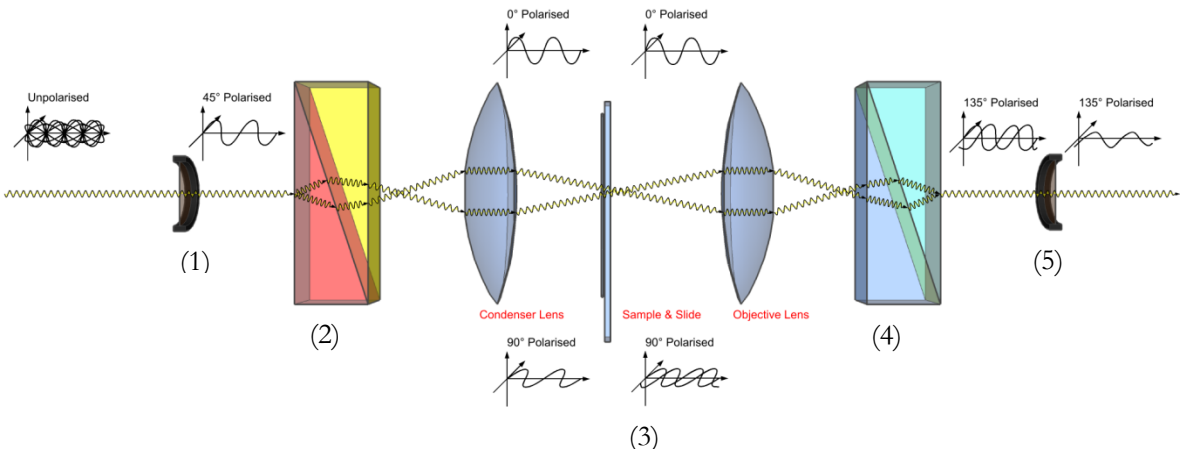

Figure 3.11: *Diagram illustrating the path of light through a differential interference contrast microscope. [14]*

From an unpolarized source of light diagonal polarized light is filtered with a linear polarizer, (1). The vertical and horizontal components are separated with a Wollaston or Nomarski Prism before passing through the sample, (2). By passing through the sample each component is shifted in its phase depending on the thickness and refractive index of the sample for each component, (3). By passing through a further prism both components are recombined and interfere with each other, (4). A second polarizer is used to remove directly transmitted light, (5). This light is imaged with a lens onto the camera. Phase shifts occur along the path light and become visible by intensity or color variations. The microscope is made by Olympus and gives possibility to generate enhanced depth of field images by moving the focus and mosaic images by moving motorized translation stage in x, y direction.

FLUORESCENCE MICROSCOPY

To investigate the deposition morphology with a higher spatial resolution fluorescence microscopy (FM) is used. Fluorescent light emitted from the sample is imaged by the FM. As UV light source a mercury vapor lamp is used. A filter allows only UV light to enter the light path of the microscope. The sample is then irradiated by UV light and fluorescence occurs. The emitted light is imaged by the microscope lens and a dichroic mirror allows UV to be reflected and emission light to be transmitted onto the detector. Another filter allows only emitted light to reach the detector.

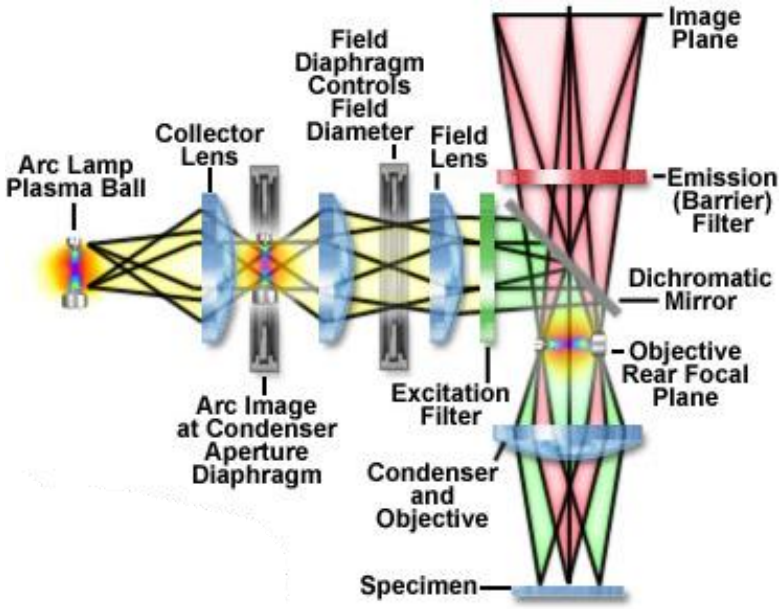

Figure 3.12: *Schematic drawing of the basic principle of a fluorescence microscope. The UV light from the mercury vapor lamp (Arc Lamp) passes the Excitation Filter. The UV light (colored green) illuminates the Specimen (or sample) and light emitted from the sample (colored red) is imaged by an objective on the Image Plane. Figure taken from [15].*

4. EXPERIMENTAL RESULTS

In this chapter the results of the experiment are presented of damage and contamination caused on four different types of samples, see **Table 4.1**. At first, with fluorescence imaging it will be shown in section 4.1 how contamination deposit is growing on each sample; first with in-situ laser-induced fluorescence imaging and later with ex-situ FM. The damage growth morphology was investigated in section 4.2 using an in-situ long distance microscope and reflection measurements. The damage growth is investigated for every sample separately and the following section 4.3 is dedicated to compare the damage threshold on HR samples. Finally in section 4.4 HR and AR coatings are compared using reflection and transmission measurements. All following tests were performed at a fluence far below the damage threshold in non-contaminated vacuum. Hence a contaminant is present on LIC tests this cause a damage on the optical samples far below the damage threshold under non-contaminated vacuum.

Coating process	Coating type	Angle of incidence	Wavelength
IBS R&D	HR	45°	355nm
MS	HR	45°	355nm
EBD	HR	45°	355nm
EBD	AR	0°	355nm

Table 4.1: *Several optical samples with different coating techniques which are used for the LIC tests are listed. Mainly HR coated samples made with IBS, MS and EBD coating process are compared. For a HR versus AR comparison EBD coated samples are used. All HR coatings are designed to work under 45° angle of incidence at 355nm. Anti-reflective coated sample is designed for perpendicular incidence.*

The substrate of every sample is made of SiO_2 as well as the top layer of the coating. The IBS R&D samples use a substrate with a rougher surface compared to other substrates. All coatings are made by Laser Optik Garbsen GmbH.

4.1. CONTAMINATION GROWTH ON HIGH-REFLECTIVE COATINGS

To allow deposit to grow without producing damage on the samples at a low fluence of 550mJ/cm² and a low contamination pressure of $5x10^{-5}$mbar are used. During LIC tests fluorescence was recorded by the fluorescence camera. **Figure 4.1** shows typical fluorescence behavior seen for EBD, MS and IBS coated samples. The total fluorescence intensity in the ROI is plotted in dependence of irradiation time.

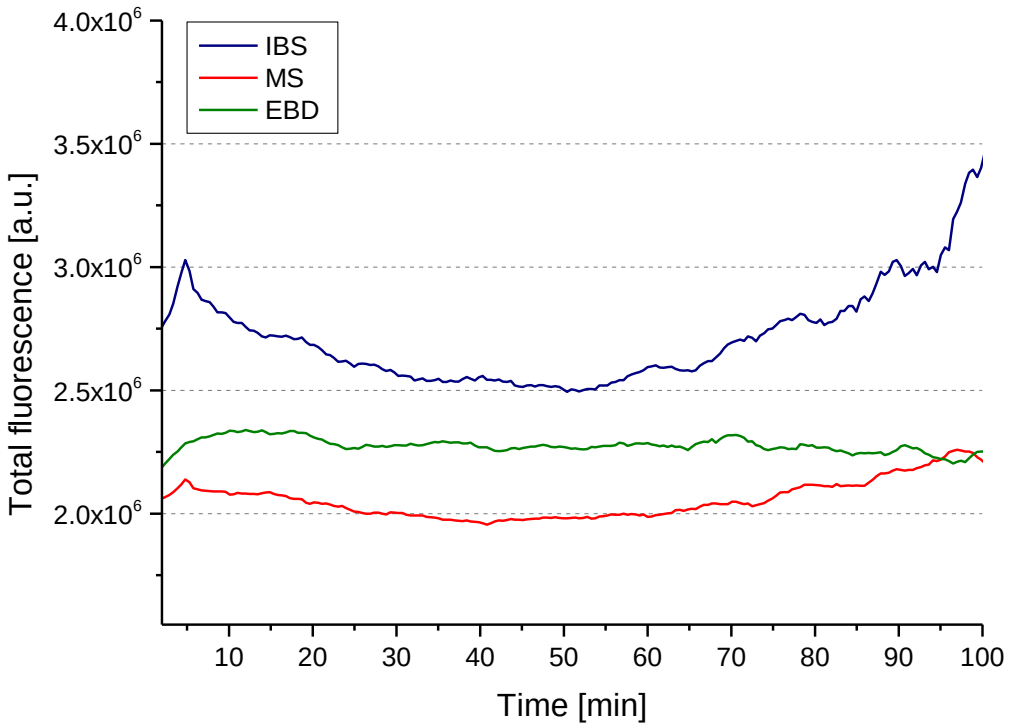

Figure 4.1: *Total fluorescence measured by in-situ laser-induced fluorescence imaging during LIC test. In comparison are HR coatings made by EBD, MS and IBS process.*

The IBS samples show highest fluorescence; hence IBS coated optics show most contamination. This was not expected since seen in **Table 2.1** IBS coatings are high quality coatings with a high damage threshold. Fluorescence is lowest on MS coatings and therefore the total amount of contamination is least. In tests with AR coated optics, EBD coatings showed also more fluorescence than MS coatings [1], see **Figure 2.2**.

The total fluorescence curves of IBS and MS samples show a similar behavior, both have a local maximum after 5min of irradiation. Between 5min and 45min irradiation time the fluorescence decreases on MS and IBS samples. Electron Beam Deposition sample do not show a significant decrease in total fluorescence.

To analyze the behavior of the growth, respectively spatial resolved contamination, samples are investigated by ex-situ FM. To investigate the growth as a function of time the laser radiation time on samples was varied on different sample positions by moving the sample holder and while keeping same contamination conditions.

Fluorescence microscopy images in **Figure 4.2** have equal magnification (20x) and exposure time of 200ms. Each image is a mosaic combined of several images of the FM by the microscope software. Top image shows fluorescence for EBD, middle for MS and bottom for IBS samples. From left to right the laser irradiation time increases from 15min up to 60min at fluence of 300mJ/cm^2 with contamination pressure of 2x10^{-5}mbar.

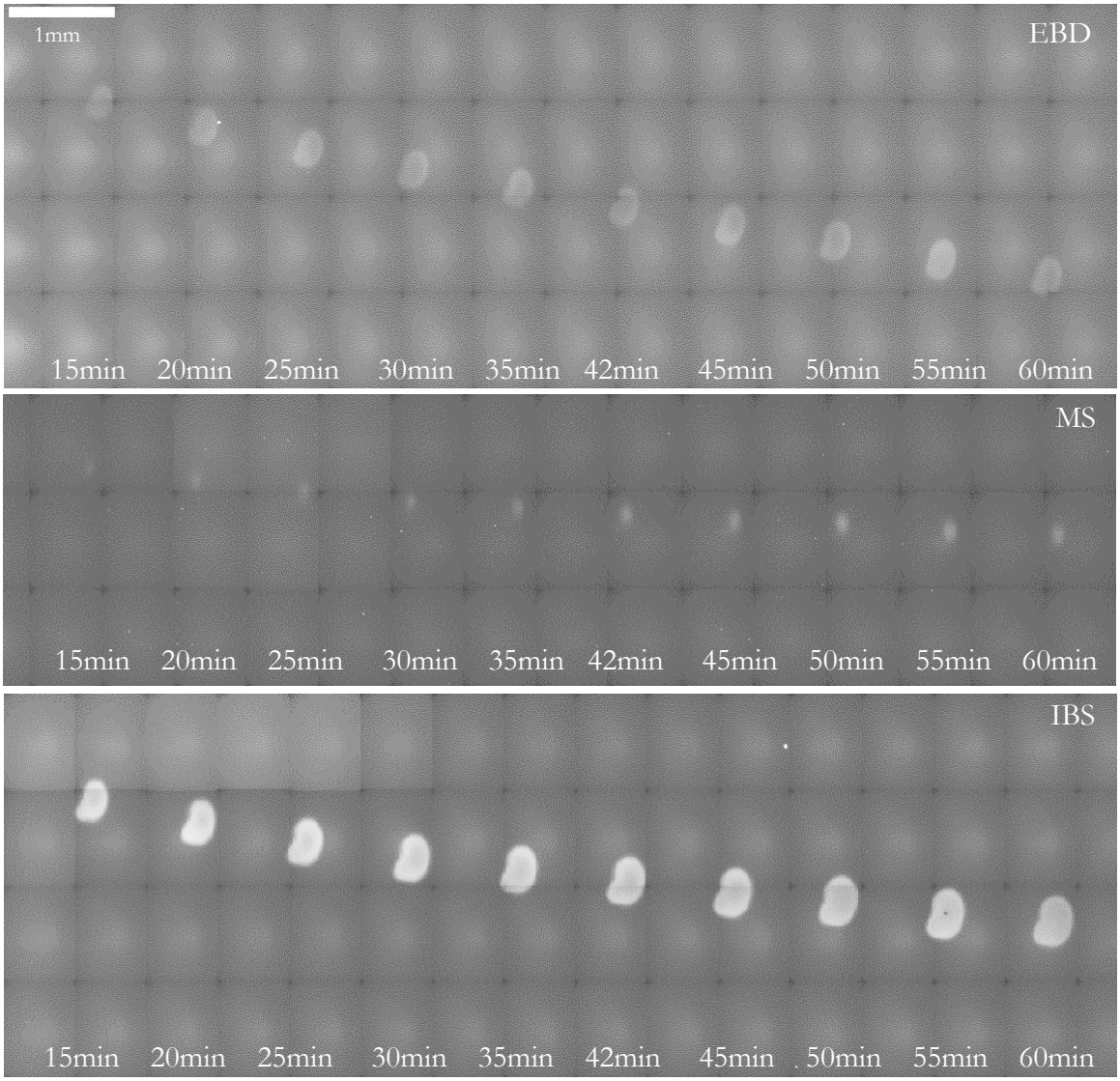

Figure 4.2: *FM mosaic image of EBD (top), MS (middle) and IBS (bottom) samples after LIC tests. Laser irradiation time varied from 15min up to 60min.*

It can be seen in **Figure 4.2** that the IBS sample shows the highest fluorescence and the MS sample the lowest. This is in agreement with the in-situ measured total fluorescence in **Figure 4.1**.

Each LIC test on each sample was recorded separately with the FM with a magnification of 20. The FM shows strong vignetting, due to inhomogeneous illumination; therefore images are post-processed to allow correct comparison. For this correction on each sample an area without any contamination was recorded under same conditions. This reference image was subtracted from each FM image of each LIC test. The following line profiles are taken from the corrected FM images through the center of the deposit in x direction. These profiles show the fluorescence level after a laser irradiation time of 15min, 45min and 75min of EBD, MS and IBS samples, see **Figure 4.3**, **Figure 4.4** and **Figure 4.5** respectively. The decrease in fluorescence intensity seen in **Figure 4.1** was reproduced with these fluorescence microscopy images.

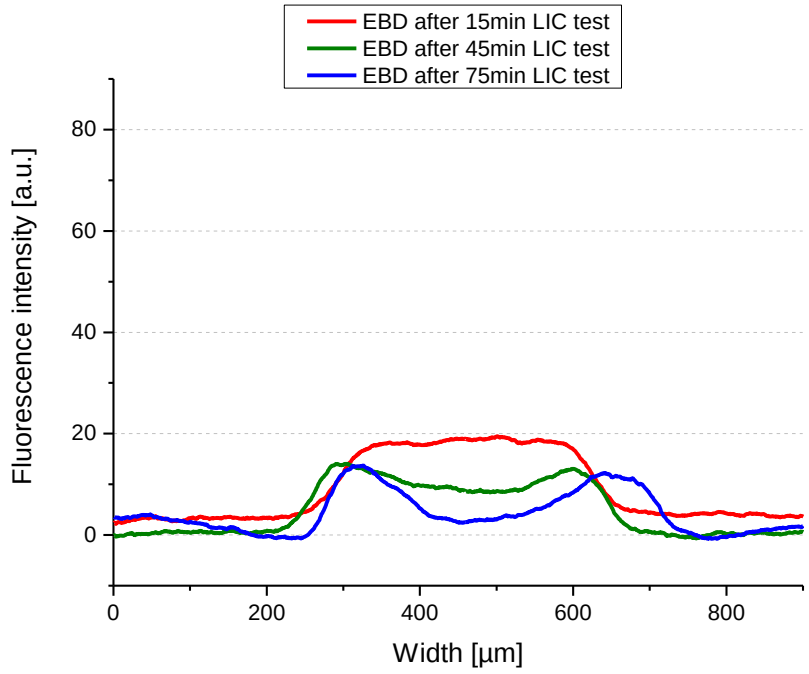

Figure 4.3: *Plot of line scans through the deposit in x direction of LIC tests after 15min, 45min and 75min. FM images from EBD sample show a transition from pancake to doughnut shape.*

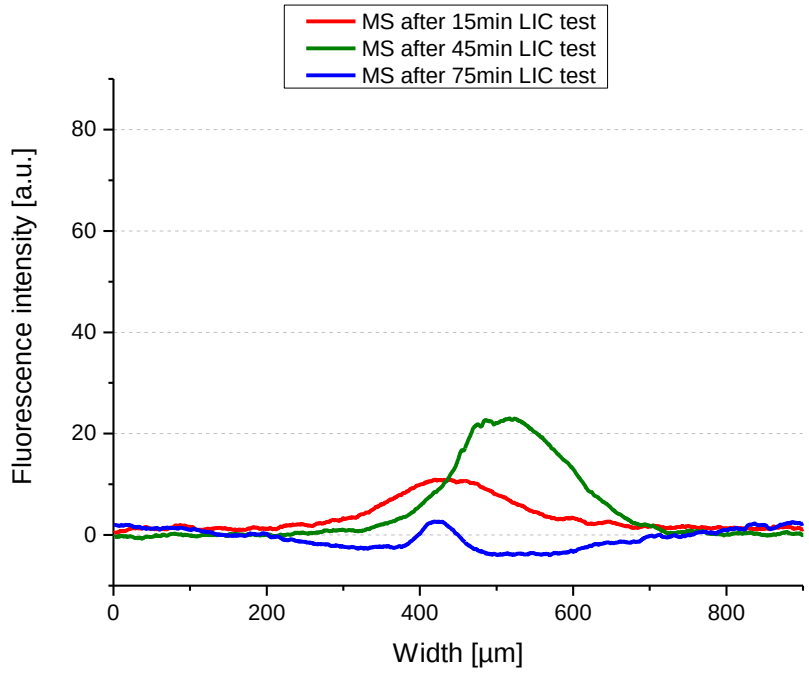

Figure 4.4: *Plot of line scans through the deposit in x direction of LIC tests after 15min, 45min and 75min. FM images from MS sample show a Gaussian shape.*

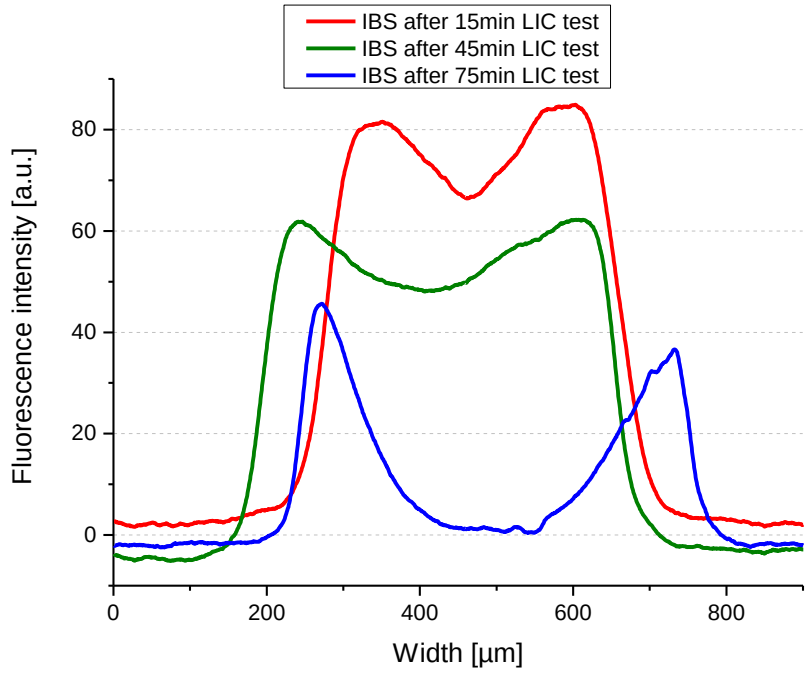

Figure 4.5: *Plot of line scans through the deposit in x direction of LIC tests after 15min, 45min and 75min. FM images from IBS sample show a doughnut shape.*

It can be seen that EBD and IBS samples show faster deposit growth as the maximum fluorescence decreases by time. Maximum fluorescence on MS samples is reached after 45min. All deposits are getting larger by time. Magnetron Sputtered samples show a higher local fluorescence in the center of the beam with 23a.u. at 45min than EBD samples with 19a.u. after 15min. Ion Beam Sputtering samples show highest local fluorescence with 85a.u. after 15min. The doughnut shaped deposit is clearly visible on EBD and IBS samples after 45min and 75min. The deposit shape of MS coated samples reminds of a Gaussian profile. The surface covered by contamination on MS samples is smaller with a diameter of about 150µm than on EBD samples with about 300µm and IBS samples with about 400µm.

Below in **Figure 4.6** is a comparison between fluorescence and DIC micrographs for EBD, MS and IBS samples after damage occurred, there is no fluorescence visible where damage occurred. These samples were irradiated for 60min with a fluence of 300mJ/cm² and a contamination pressure of 8.5×10^{-5}mbar.

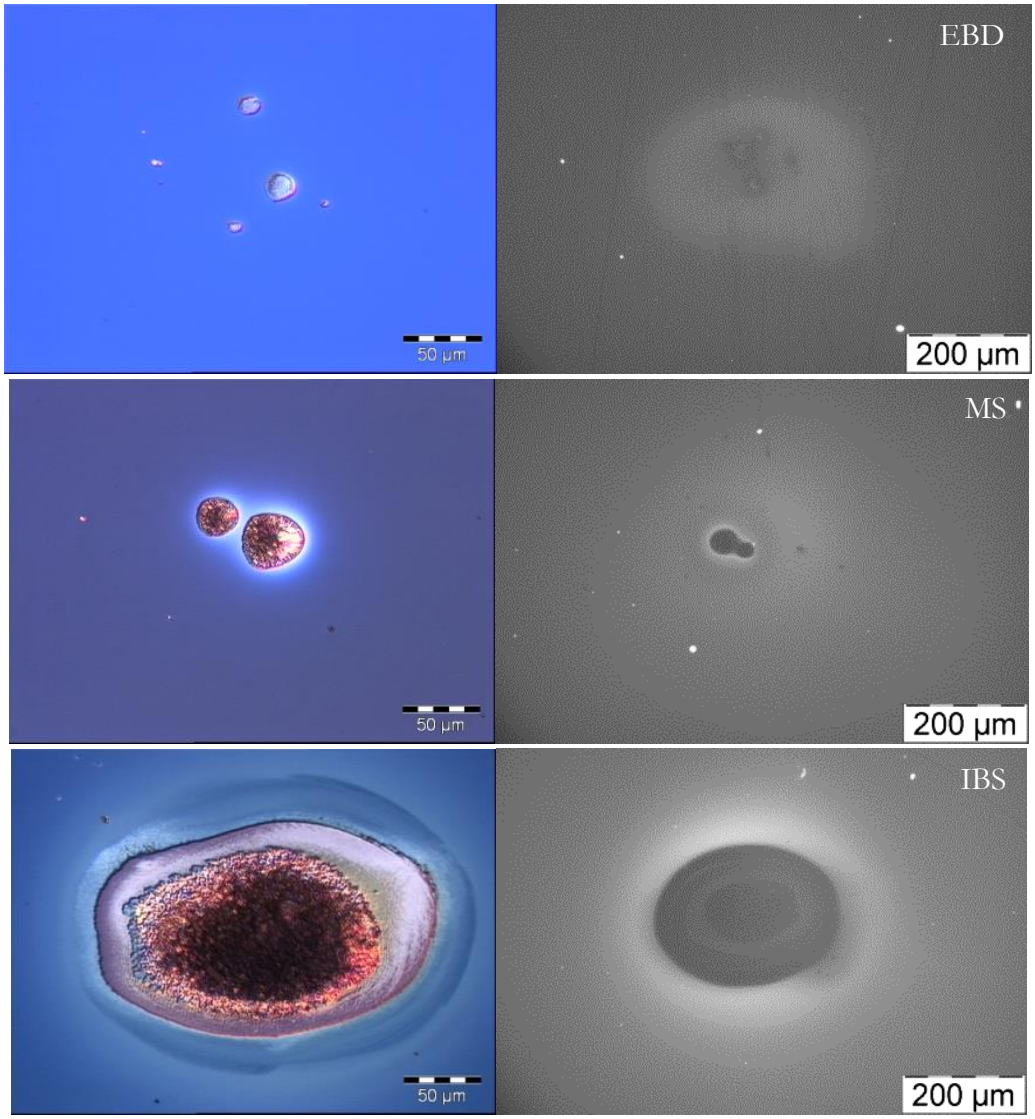

Figure 4.6: *DIC micrograph (left) and FM micrograph (right) in comparison of each sample after 60min LIC test. From top to bottom: EBD, MS and IBS samples are shown.*

CONCLUSION

It was seen that the contamination on IBS samples is highest. The area covered by contamination and the amount of contamination was higher compared to EBD and MS samples. MS samples show a lower total amount of contamination than IBS and EBD samples due to a smaller contaminated area. Higher local fluorescence intensity on MS samples show a thicker deposition than on EBD samples. Electron Beam Deposition samples show the thinnest deposition compared to IBS and MS. But the contaminated area was larger compared to MS.

4.2. CONTAMINATION INDUCED DAMAGE MORPHOLOGY ON HIGH-REFLECTIVE COATINGS

In this section images taken with the long distance microscope are shown for following samples: EBD, MS and IBS. Samples are investigated at a low and high fluence. The long distance microscope records one sample during a LIC test to investigate damage growth. At first a look is taken with the long distance microscope on each sample showing a relation between a decreasing reflection and occurrence of damage. The test conditions (contamination pressure and fluence) for each of the two LIC tests with different samples were similar, so that results are comparable. A DIC micrograph shows the damage after the LIC test with a higher resolution.

ELECTRON BEAM DEPOSITION

It takes a long time on EBD samples after first sign of damage becomes visible after 10h. It was tested with a fluence of 400mJ/cm² and contamination pressure of 3.1×10^{-5}mbar. A couple of spots appear with a size of about 10µm each. This has only a slight effect on the reflection loss, which decreased to 98%. Those small damages appear to start at almost the same time and are spread within an area of 200µm x 250µm. These small spots merge until they form a large damaged area after 24h.

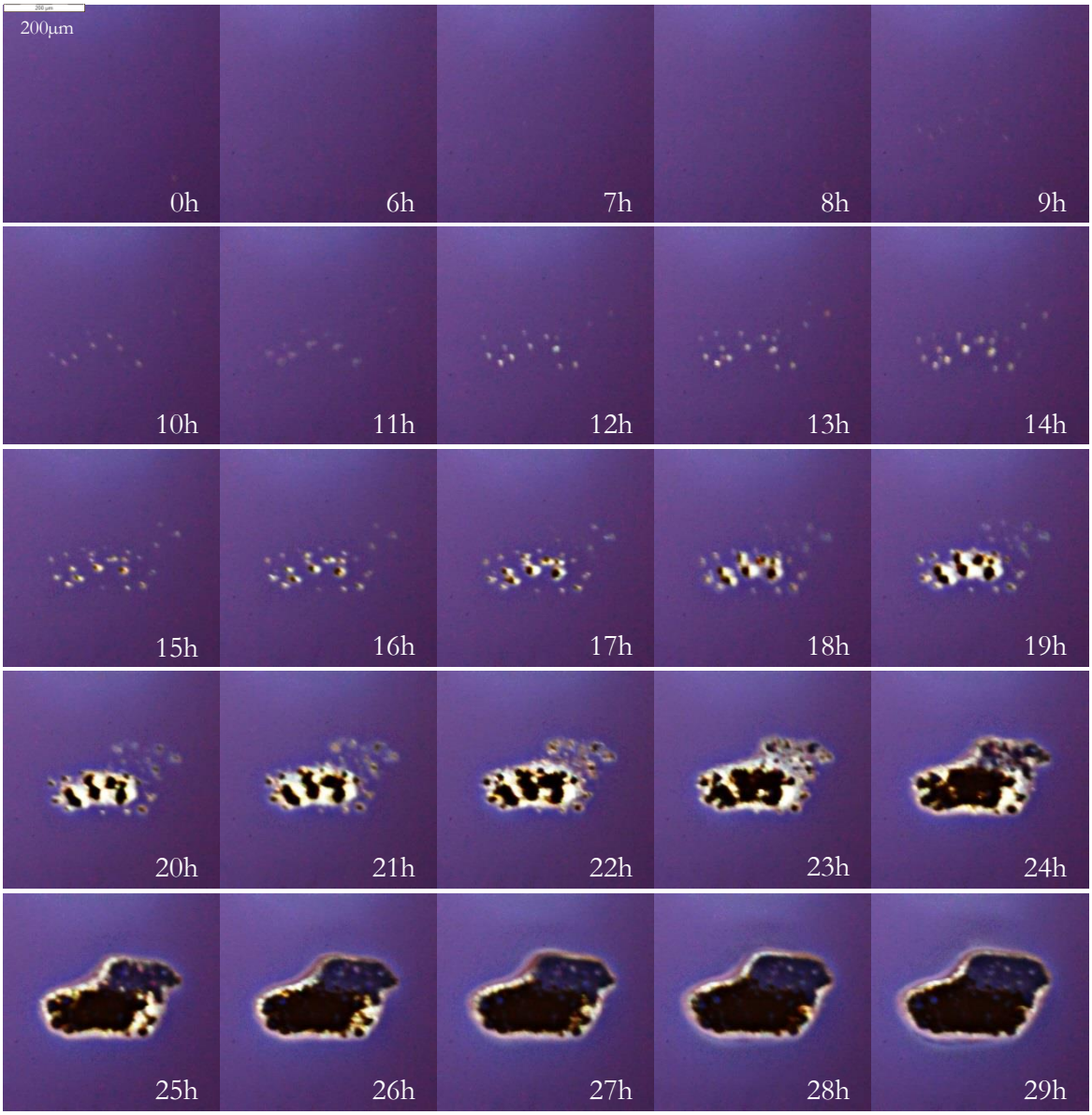

Figure 4.7: *In-situ long distance microscope images of EBD sample during LIC test. Test conditions are H_P=400mJ/cm² with a contamination pressure of 3.1×10^{-5} mbar.*

After the LIC test was performed a DIC image was taken which can be compared to image taken with the long distance microscope after 29h, **Figure 4.8**.

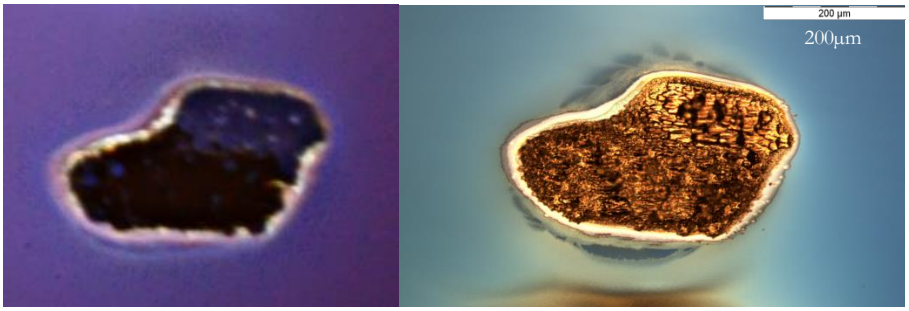

Figure 4.8: *In-situ long distance microscope image (left) taken after 29h in comparison with DIC micrograph (right) of EBD sample taken after LIC test.*

After an irradiation time of 10h reflection decreased slightly to 98%, damage becomes visible with the long distance microscope. Small spots grow by time resulting in a reflection decrease down to 88% after 16h. Those spots grown together and after 20h the reflection decreased down to 56%.

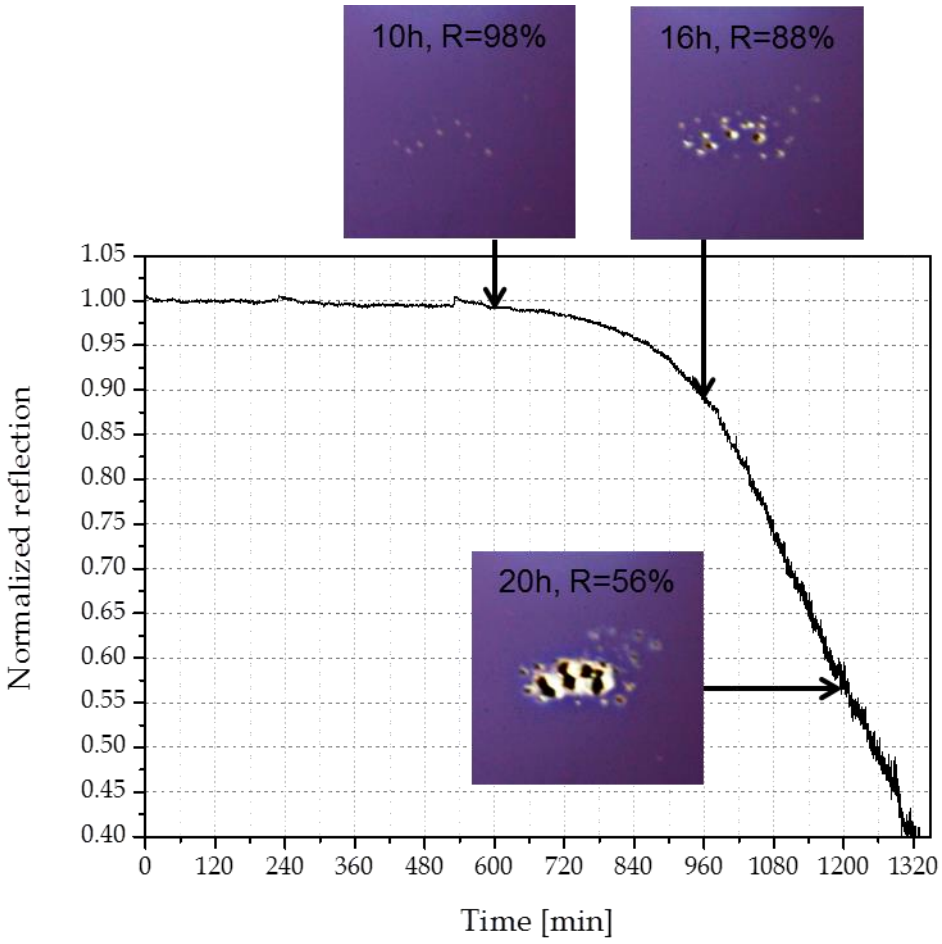

Figure 4.9: *Normalized reflection measurement of the EBD sample during a LIC test, from measurement seen in* ***Figure 4.7****.*

MAGNETRON SPUTTERING

The MS coated optic was tested at a fluence of 660mJ/cm² and a contamination pressure of $1x10^{-5}$mbar. The Magnetron Sputtered samples show a different contamination shape than IBS and EBD samples, see **Figure 4.4**. But the damage morphology is similar to EBD samples, seen in **Figure 4.7**. Damage starts to occur with a couple of small spots within an area of 200µm x 250µm after 8h. The reflection decreased just slightly about 1%. Those spots are about 10µm in diameter and getting larger by time until they merge after 22h with a decrease of the reflection down to 85%.

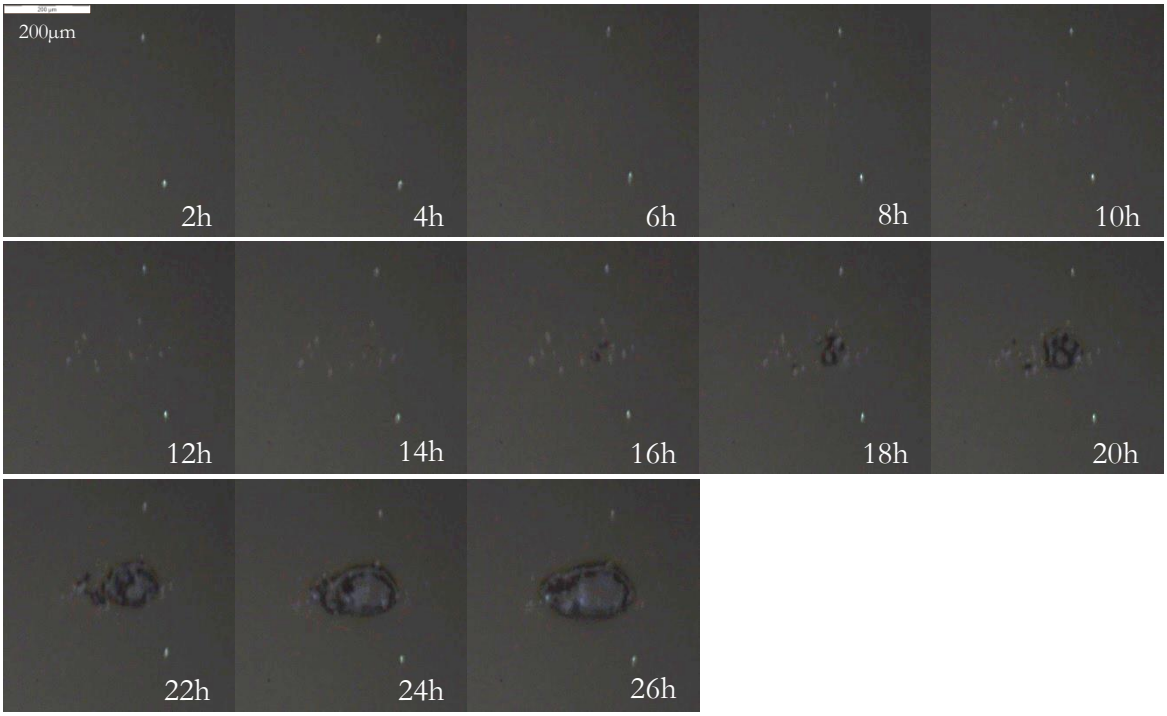

Figure 4.10: *In-situ long distance microscope images of MS sample during LIC test. Test conditions are at a fluence of 660mJ/cm² with a contamination pressure of 1×10^{-5} mbar.*

After the LIC test was performed a DIC image was taken which can be compared to an image taken with the long distance microscope after 26h, see **Figure 4.11**.

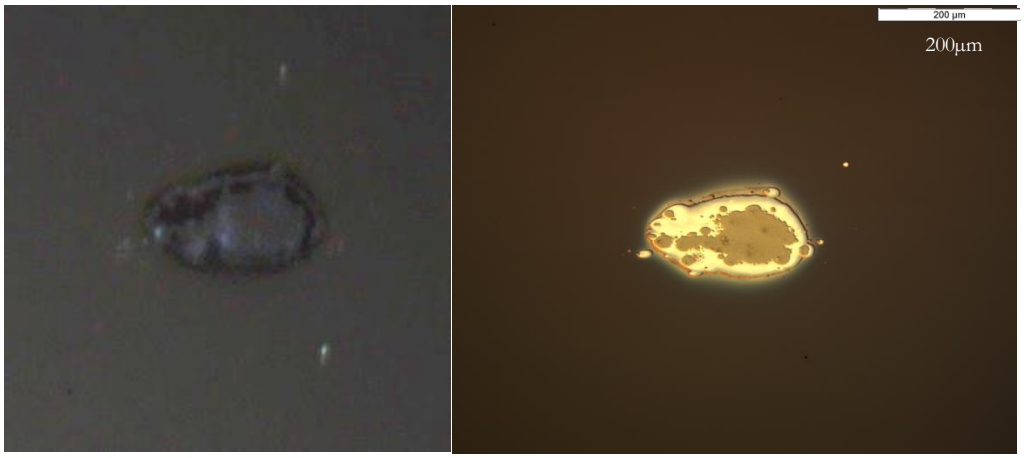

Figure 4.11: *In-situ long distance microscope image (left) taken after 26h in comparison with DIC micrograph (right) of MS sample taken after LIC test.*

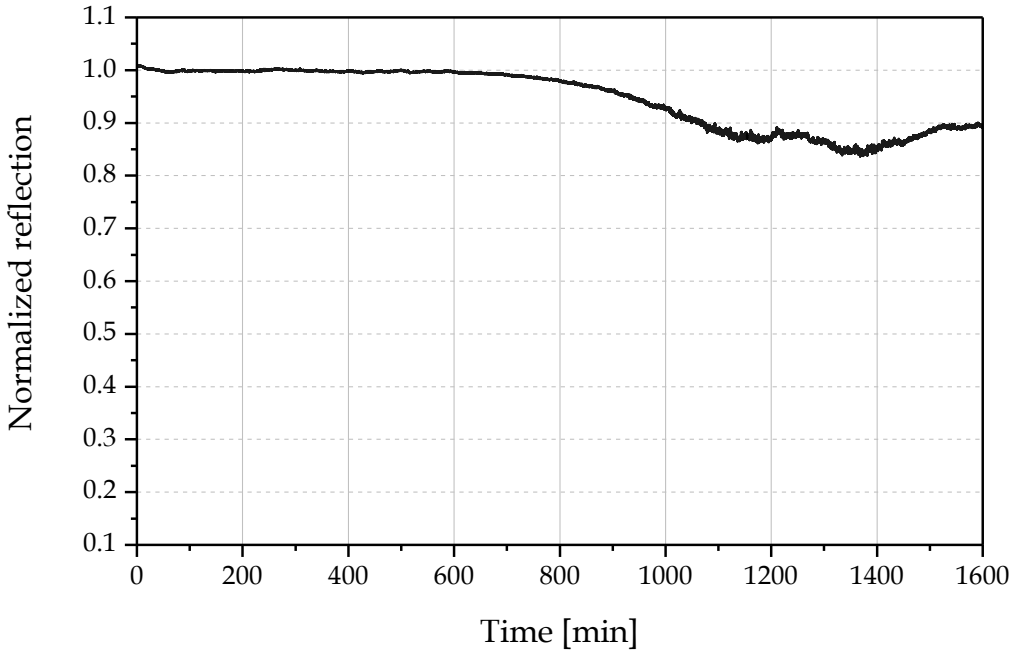

Figure 4.12: *Normalized reflection measurement of the MS sample during a LIC test, from measurement seen in* ***Figure 4.10****.*

ION BEAM SPUTTERING

In the following LIC test at a fluence of 360mJ/cm² and a contamination pressure of $3.5x10^{-5}$mbar the IBS sample shows damage which is visible after 15min (see **Figure 4.13**) with a decrease of the reflection by 1%. The damage starts from the center of the beam and getting larger by time. After 30min it is about 100µm in diameter with reflection decreased by 8%.

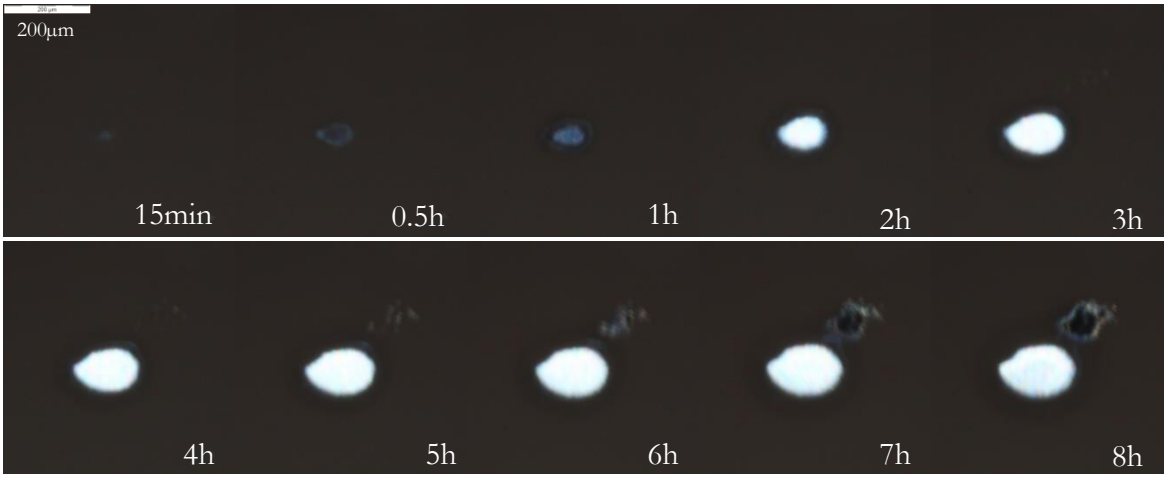

Figure 4.13: *In-situ long distance microscope images of IBS sample during LIC test. Test conditions are H_P=360mJ/cm² with a contamination pressure of $3.5x10^{-5}$ mbar.*

After the LIC test was performed a DIC image was taken which can be compared to an image taken with the long distance microscope after 8h, **Figure 4.14**.

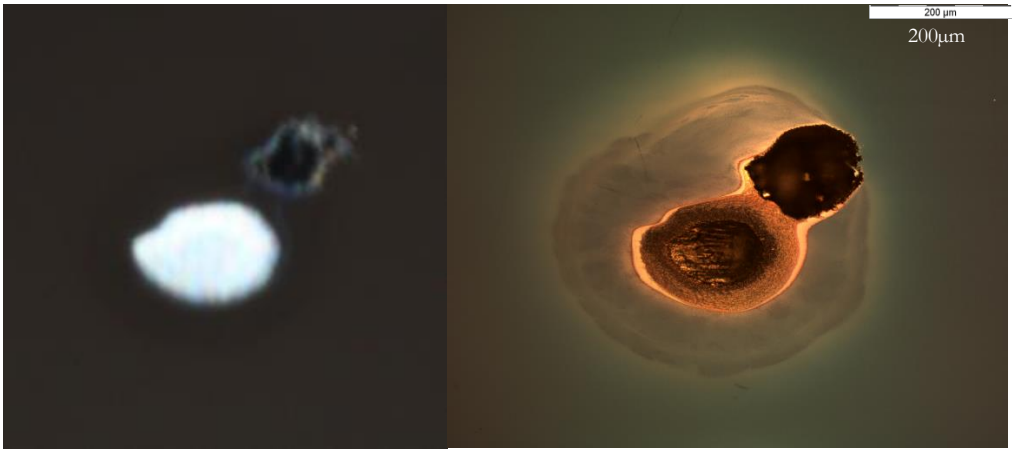

Figure 4.14: *In-situ long distance microscope image (left) taken after 8h in comparison with DIC micrograph (right) of IBS sample taken after LIC test. The damage has a diameter of about 500µm.*

Reflection decreases very quickly in time testing IBS coating, **Figure 4.15**.

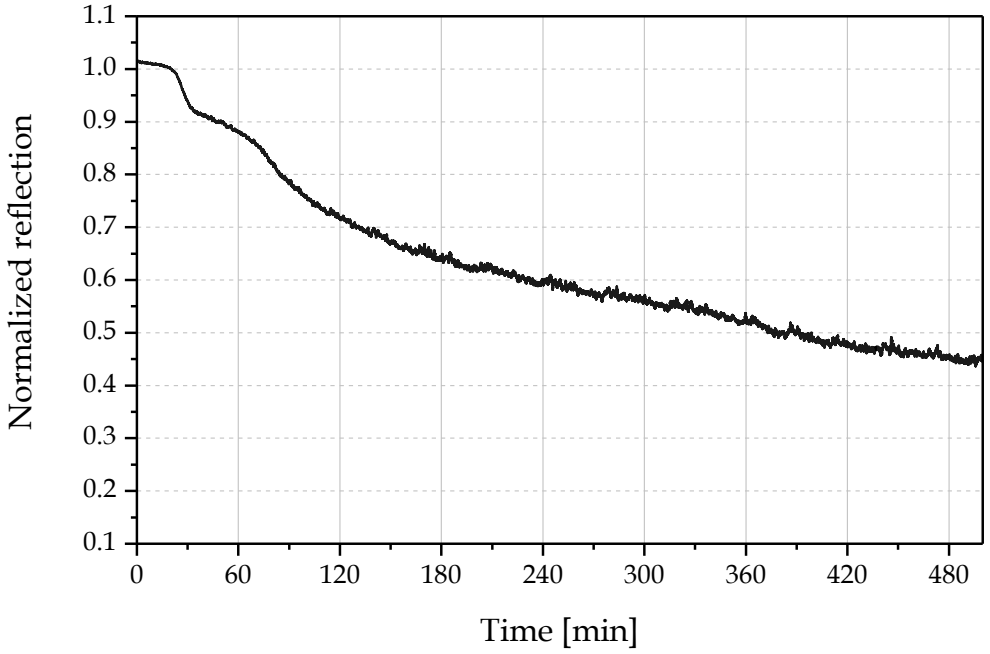

Figure 4.15: *Normalized reflection measurement of the IBS sample during a LIC test, from measurement seen in* ***Figure 4.13****.*

These three tests have shown that a decrease of the reflection by 1% produces small damages of a few dozens of µm in diameter. After a decrease of the reflection by 10% the damage is much more significant.

On other LIC tests which were interrupted before the reflection decreased significantly, small localized damage spots could be found on DIC microscope images. Damages with a spot size of few µm are found; see **Figure 4.16** (left). Those localized damages getting larger until they grow together, see **Figure 4.16** (right).

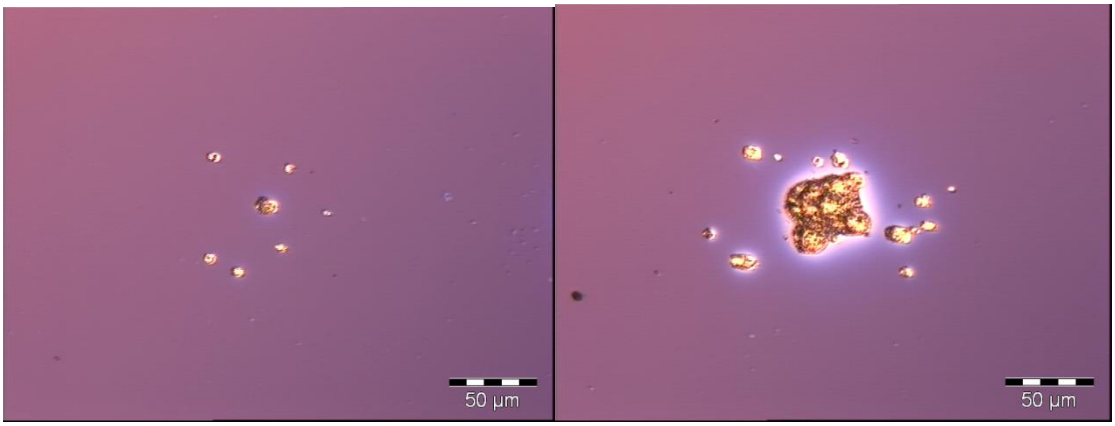

Figure 4.16: *Localized damages on MS samples after LIC test with 75min (left) and 95min (right) irradiation time. Test conditions are a fluence of 262mJ/cm² with a contamination pressure of 4.8x10⁻⁵mbar.*

EXPOSITION TO HIGH FLUENCE

Electron Beam Deposition

The fluence was three times higher at 1250mJ/cm² than on previous LIC test using the EBD sample (**Figure 4.7**). This causes a much faster damage, after 70min reflection decreased by 10%. Just two localized damages are visible in the following long distance microscope images, **Figure 4.17**. The LIC test was performed at a contamination pressure of $4x10^{-5}$mbar.

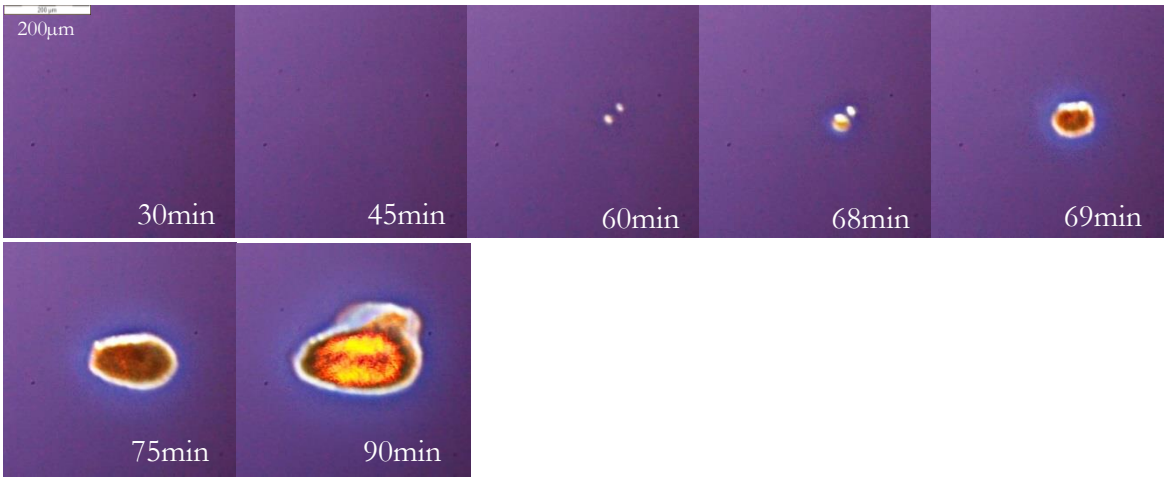

Figure 4.17: *In-situ long distance microscope images of EBD sample during LIC test. Test conditions are H_P=1250mJ/cm² with a contamination pressure of 4x10⁻⁵mbar.*

After the LIC test was performed a DIC image was taken which can be compared to an image taken with the long distance microscope after 90min, see **Figure 4.18**.

Figure 4.18: *DIC micrograph of EBD sample after 90min LIC test.*

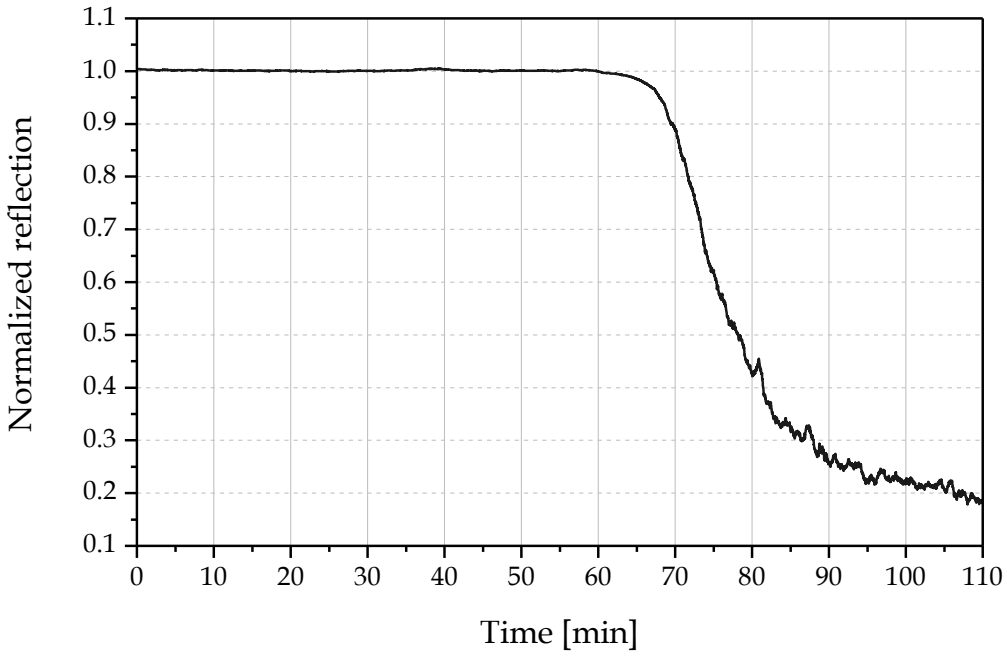

Figure 4.19: *Normalized reflection measurement of the EBD sample during a LIC test, from measurement seen in* ***Figure 4.17****.*

Magnetron Sputtering

The LIC test was performed on a MS sample at a fluence of 1050mJ/cm² and contamination pressure of $4x10^{-5}$mbar. Fluence was 1.6 times higher than in a previous LIC test on MS sample, (**Figure 4.10**) and a difference in damage morphology is visible again. Damage forms mainly at the center of the beam. Localized damages occur after 105min but are not that significant than under lower fluence.

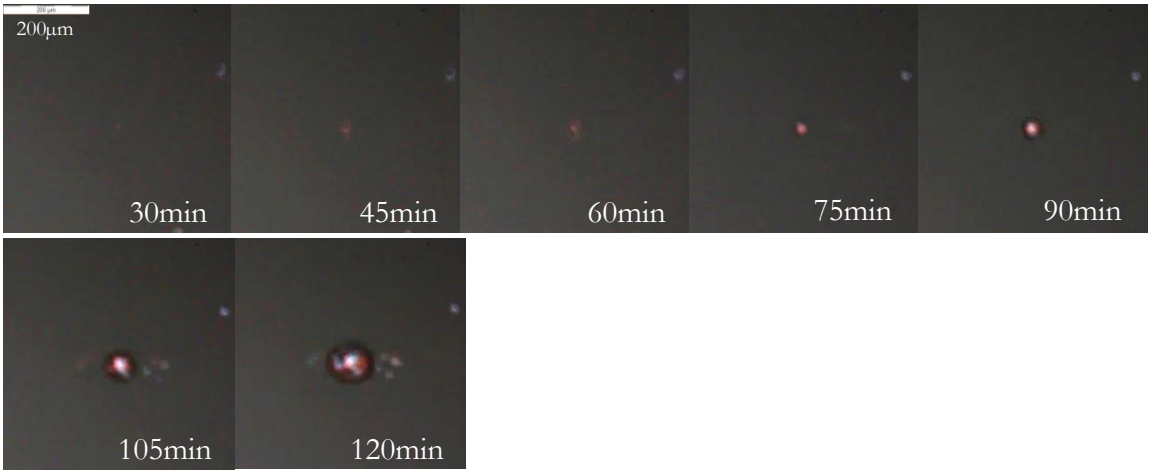

Figure 4.20: *In-situ long distance microscope images of MS sample during LIC test. Test conditions are a fluence of 1050m]/cm² with contamination pressure of 4×10^{-5} mbar.*

After the LIC test was performed a DIC image was taken which can be compared to an image taken with the long distance microscope after 120min, see **Figure 4.21**.

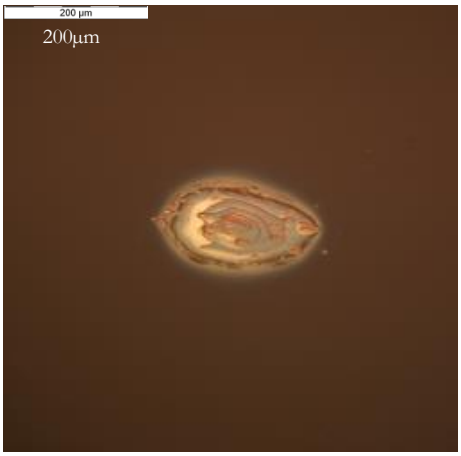

Figure 4.21: *DIC micrograph of MS sample after 120min LIC test.*

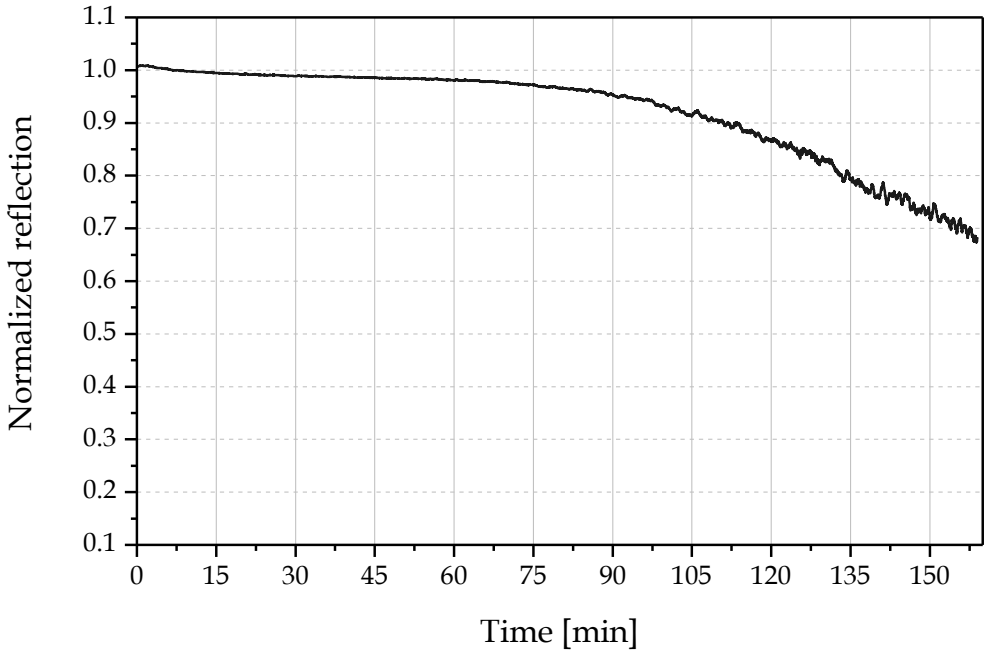

Figure 4.22: *Normalized reflection measurement of the MS sample during a LIC test, from measurement seen in* ***Figure 4.20****.*

Ion Beam Sputtering

The LIC test on IBS sample at a fluence of 740mJ/cm² is two times higher than previously (**Figure 4.13**) and under a contamination pressure of $3.5x10^{-5}$mbar showing the same damage morphology.

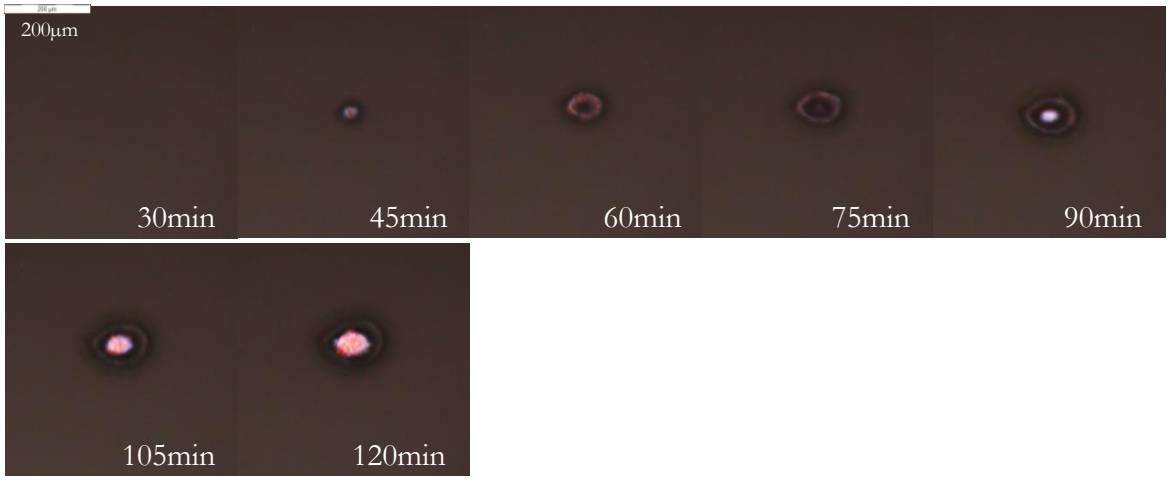

Figure 4.23: *In-situ long distance microscope images of IBS sample during LIC test. Test performed with a fluence of 740mJ/cm² and contamination pressure of $3.5x10^{-5}$ mbar.*

After the LIC test was performed a DIC image was taken which can be compared to an image taken with the last long distance microscope after 120min, see **Figure 4.24**.

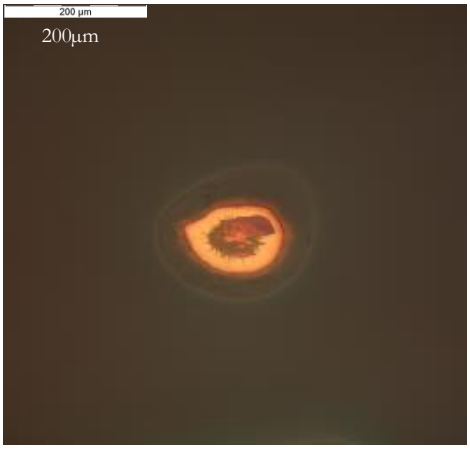

Figure 4.24: *DIC micrograph of IBS sample after LIC test.*

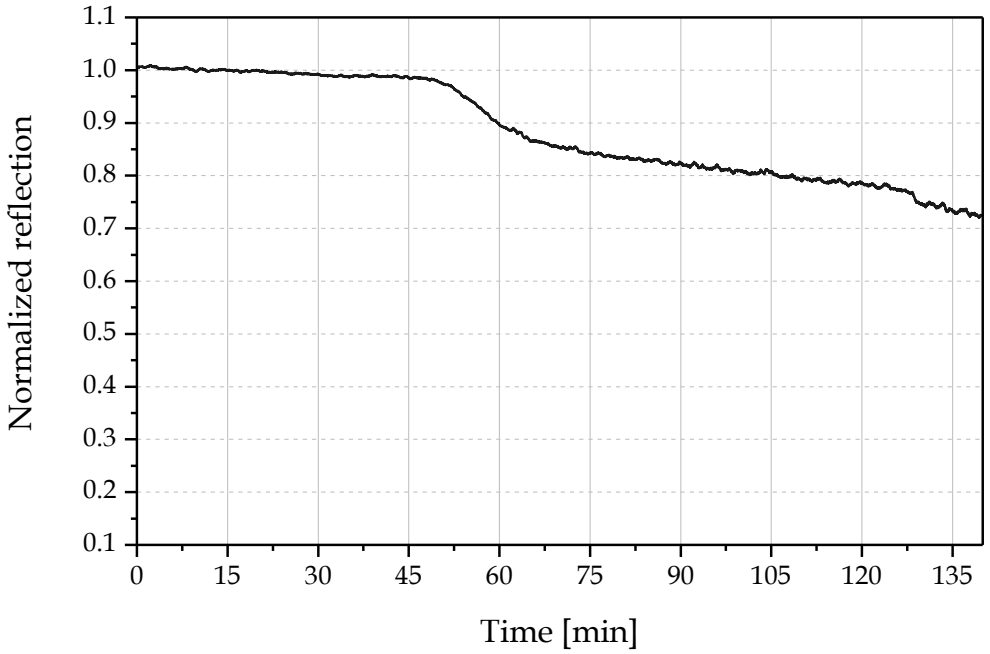

Figure 4.25: *Normalized reflection measurement of the IBS sample during a LIC test, from measurement seen in* ***Figure 4.23****.*

Damage morphology on the IBS samples do not change. Under higher fluence it is visible that morphology changes on EBD and MS samples. Fewer small spots are visible when damage starts to occur on MS and EBD samples.

Results are showing that damages on IBS samples always start where the center of the beam irradiates the optical surface and becomes larger by time. MS and EBD samples show localized damages.

EX-SITU INVESTIGATION

Ex-situ DIC microcopy gives a more detailed view on damages. In **Figure 4.26** damages are compared with ex-situ and DIC microscope. Samples are tested under a contamination pressure of $4x10^{-5}$mbar and irradiated at a fluence of 1050mJ/cm² for 60min.

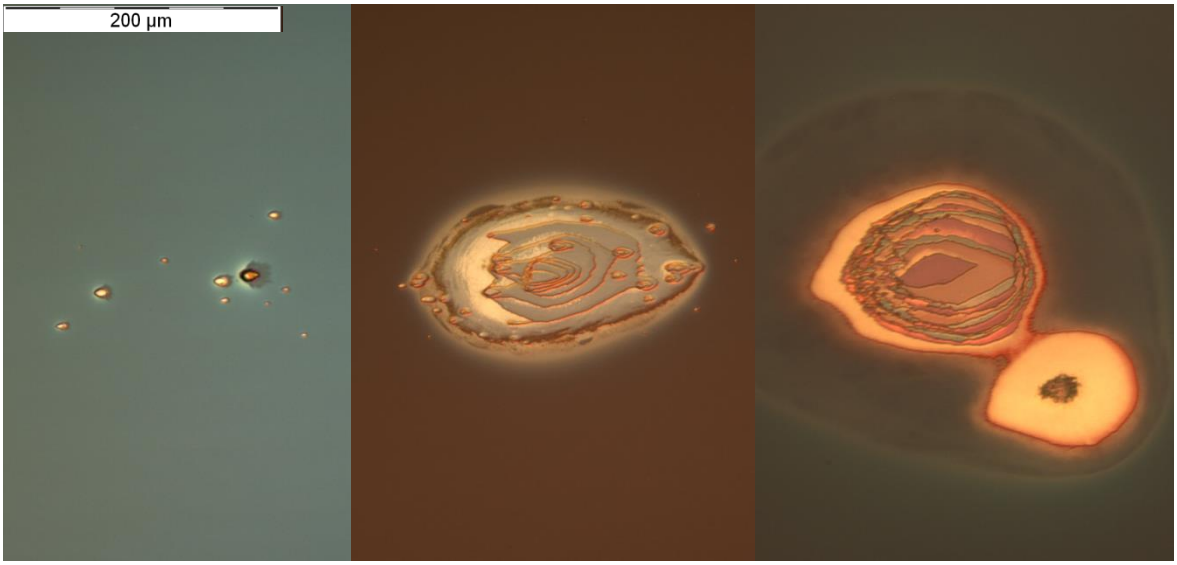

Figure 4.26: *Ex-situ DIC micrographs after LIC test of EBD (left), MS (middle) and IBS (right) samples.*

On the EBD sample 10 localized damages with a minimum diameter of 2.5µm and maximum diameter of 15µm are detected. The spots are spread around an area of 150µm x 200µm. Damage on the MS sample is stronger with several damaged layers of the HR coating. The damage has the same diameter than the damage on the EBD sample with 150µm x 200µm. On the MS sample it is visible that damage starts with localized spots as well. The IBS sample shows the largest damage with a diameter of 260µm. Damage on those three samples do not affect all HR coating layers. On the following longer LIC test the substrate surface was damaged even on the EBD sample, **Figure 4.27**. The LIC test was run for 6h at a fluence of 700mJ/cm² and a contamination pressure of $3.5x10^{-5}$mbar.

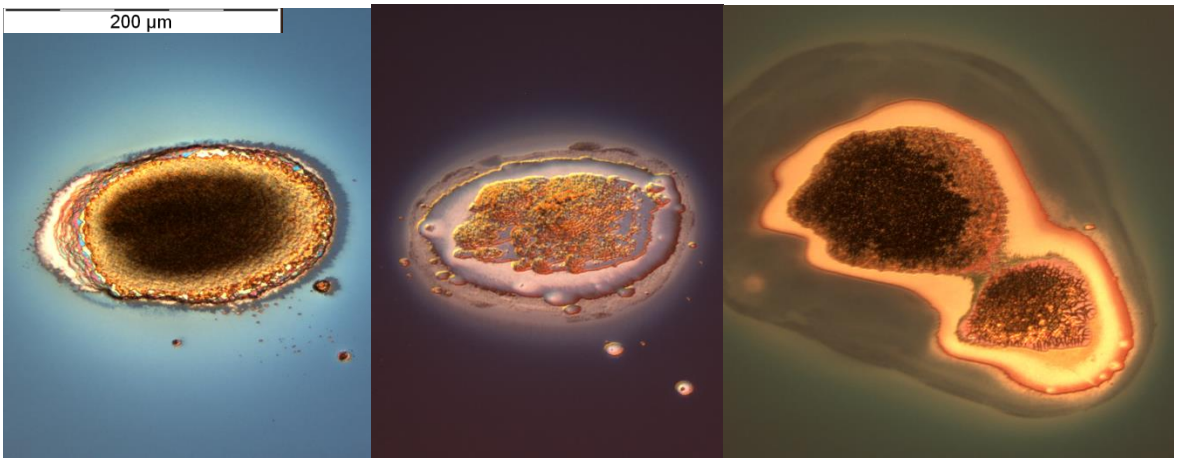

Figure 4.27: *Ex-situ DIC micrographs after LIC test of EBD (left), MS (middle) and IBS (right) samples.*

Damage on the EBD sample has a diameter of 205µm and on the MS sample of 194µm. It can be seen that the damage on the IBS sample is largest with a diameter of 285µm. On every sample small spots of localized damages can be found with DIC microscope. In **Figure 4.27** (right) they can be found on the IBS sample as well close to the edge of the damage.

On some damaged samples separate layers from the HR coating are visible down to the substrate, see **Figure 4.28**.

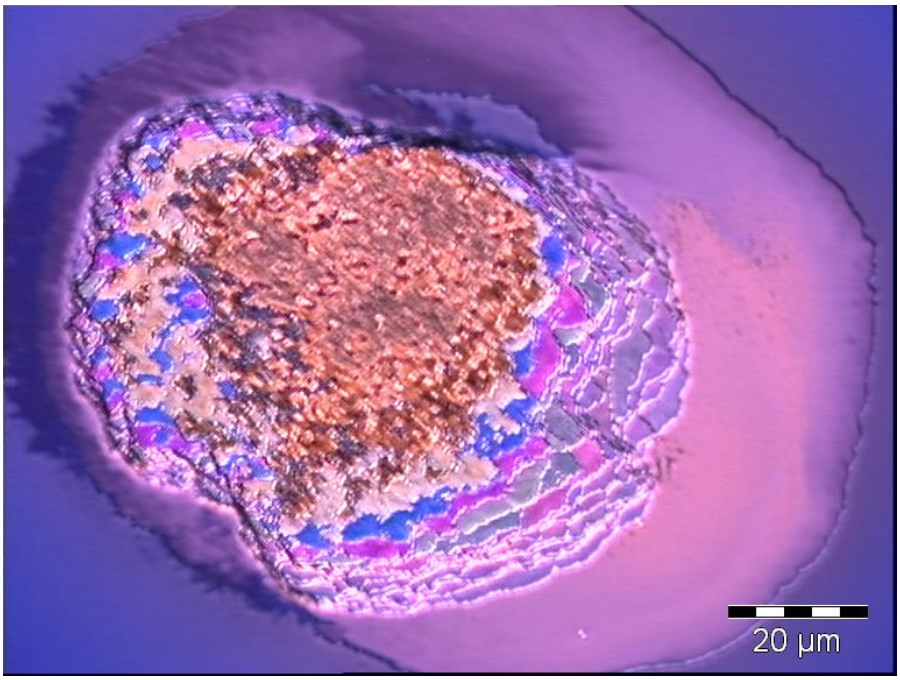

Figure 4.28: *HR EBD sample damage after LIC test. About 15 layers of the HR coating are visible. The damage is about 1.6µm in depth.*

4.3. CONTAMINATION INDUCED DAMAGE THRESHOLD ON HIGH-REFLECTIVE COATINGS

To determine the point in time where damage occurs reflection measurements are used. With in-situ reflection measurements it is possible to investigate all samples simultaneously under same conditions. Previous measurements in section 4.2 have shown that a loss in reflection follows a surface damage. This is why damages can be compared using reflection measurements. Further reflection measurements show a dependence of contaminant pressure and fluence of the laser. It is expected that IBS samples show lowest damage threshold compared to EBD and MS samples, due to largest and highest amount of contamination. And due to lowest local amount of contamination on EBD samples it is to expect that EBD samples show a higher damage threshold than IBS and MS samples.

DEPENDENCE OF FLUENCE

To determine occurrence of damages as a function of the fluence, LIC tests with three different fluences are performed. Samples are irradiated at different positions by moving the translation stage of the sample holder while keeping same contamination conditions. In following graphs dependence of fluence on EBD, MS and IBS samples are shown in **Figure 4.29**, **Figure 4.30** and **Figure 4.31**. The LIC test was performed for a duration of 60min at a contamination pressure of 1.5×10^{-4}mbar ±15%.

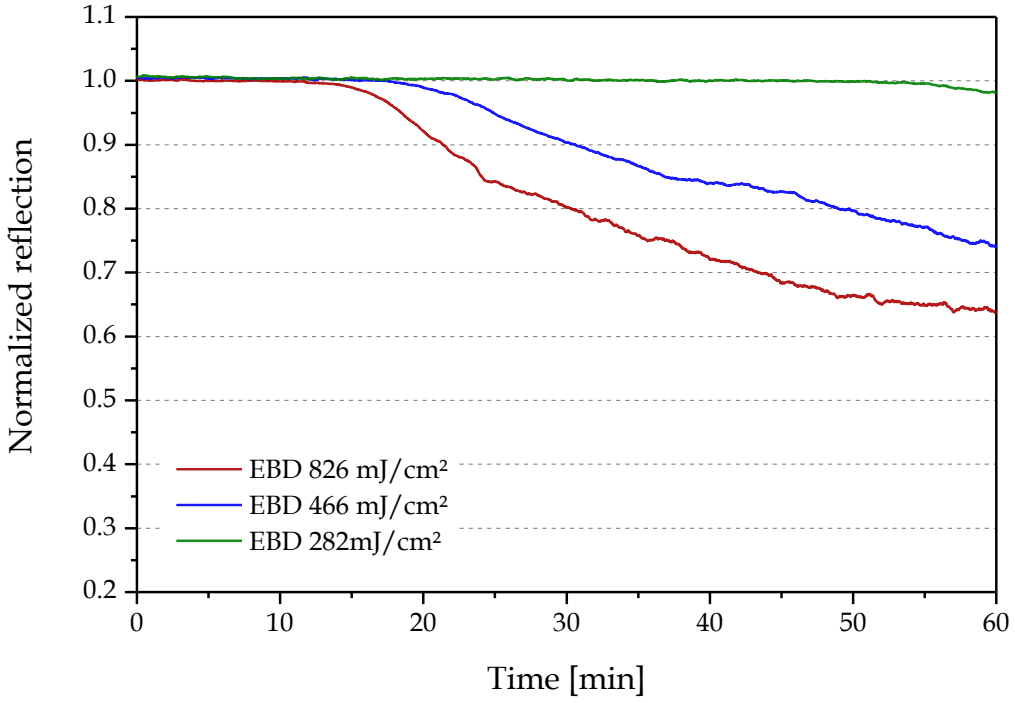

Figure 4.29: *Normalized reflection during LIC test of EBD in dependence of fluence.*

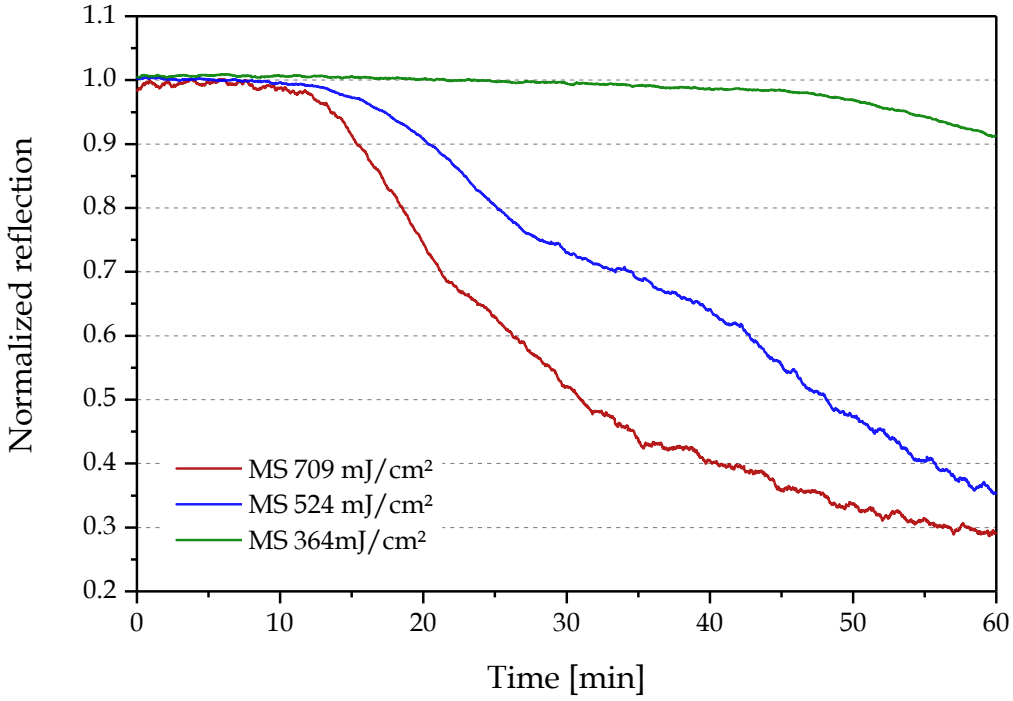

Figure 4.30: *Normalized reflection during LIC test of MS in dependence of fluence.*

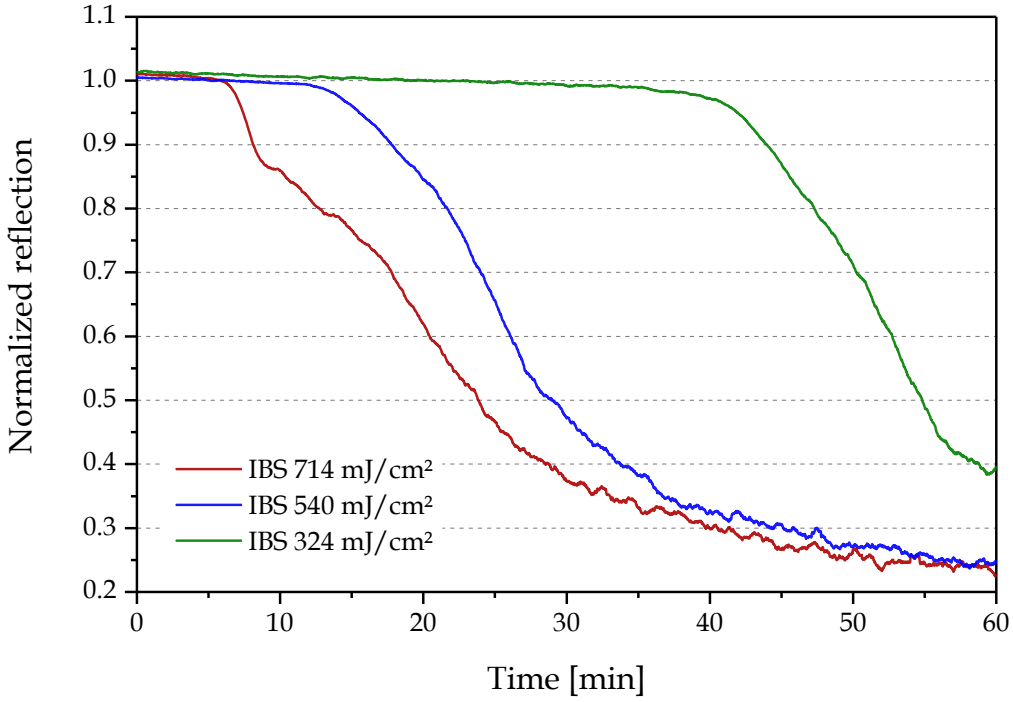

Figure 4.31: *Normalized reflection during LIC test of IBS in dependence of fluence.*

It can be seen that under higher fluence the damage occurs earlier.

COATING COMPARISON

In **Figure 4.32** a direct comparison is shown between EBD, MS and IBS samples under a contamination pressure of $1.1x10^{-4}$ mbar and a mean peak fluence of 750mJ/cm². It can be seen that the reflectivity on IBS samples decreases quickly, after 7min the reflection decreases below 95%. The EBD samples are always the last samples where reflection decreases, in this test the reflection decreased below 95% after 18min. Reflection on the MS samples decreases below 95% after 14min. Ex-situ investigations could verify that damage occurred.

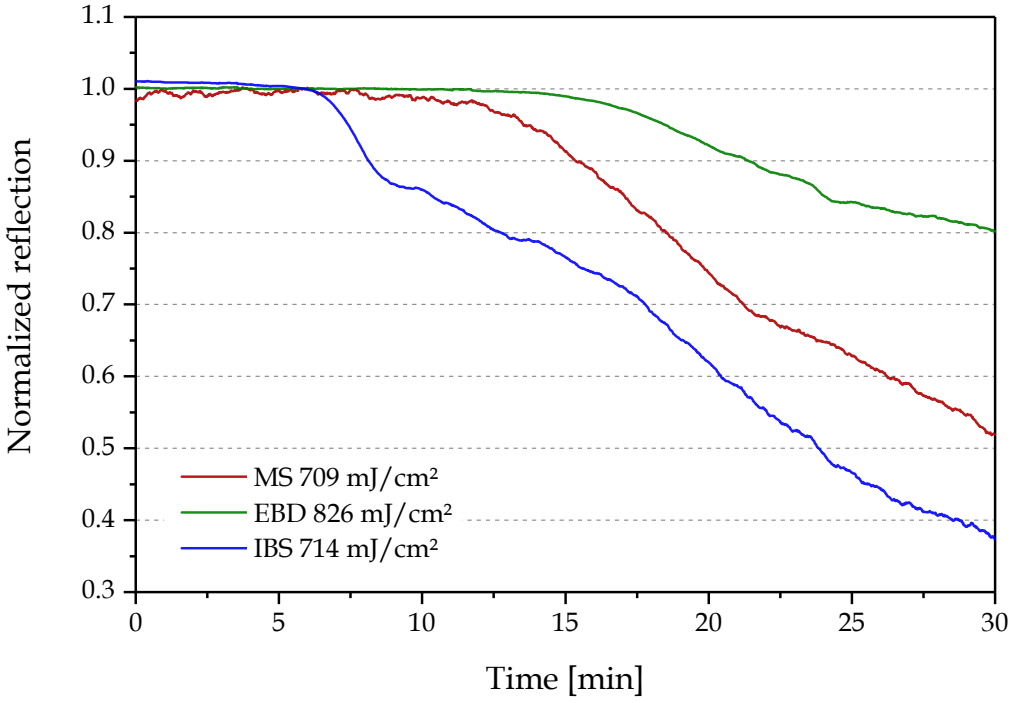

Figure 4.32: *Normalized reflection of HR optics as function of irradiation time. Contamination pressure was $1.1x10^{-4}$ mbar with a peak fluence of 750mJ/cm².*

In all reflection measurements where EBD, MS and IBS samples are directly compared it was seen that EBD samples always performed best and IBS samples always worst. In the following section those results are investigated as a function of the fluence and contamination pressure.

BREAK POINT

In the previous chapter it was shown that contamination and damage depend on the contamination pressure and fluence. Several tests under different conditions for damage behaviors were performed and below in **Table 4.2** are listed all measurements where damage occurred. To compare these test results the break point was defined as the point in time where the reflection decreases down to 95%. Below a reflection of 95% damages becomes visible.

internal Test	**Pressure [mbar]**	**Fluence [mJ/cm²] ±5 mJ/cm²**			**Break point [min] ± 1min** (Reflection decrease to 95%)		
#	naphthalene	EBD	MS	IBS	EBD	MS	IBS
5	8.5^{-5}	282	364	324	65	55	42
6	1.2^{-4}	467	524	540	25	17	15
7	1.1^{-4}	826	709	714	18	14	7
8	9.0^{-5}	766	888	909	>60	28	7
9	9.0^{-5}	960	1061	1068	36	38	6
36	1.5^{-5}	1149	994	1026	>60	>60	18
37	3.5^{-5}	566	489	506	>230	>230	170
38	2.2^{-5}	833	720	745	>120	>120	55
39	6.2^{-5}	1148	1018	1027	65	55	10
42	4.2^{-5}	1034	895	924	155	127	22
43	4.3^{-5}	1293	1118	1155	68	28	6
44	3.1^{-5}	402	348	359	870	470	205
45	1.1^{-5}	801	668	611	1100	930	48

Table 4.2: *Break point of EBD, MS and IBS sample in dependence of contamination pressure and fluence.*

It can be seen that the IBS samples are always the first samples where reflection decreases to 95% followed by the MS samples. The EBD samples always show highest Break point time. If '>' is in front of the break point time than reflection has not decreased below 95% during the LIC tests and no damage occurred within this time.

Contour plots show how the break point of EBD, MS and IBS samples depend on the fluence and contamination pressure as shown in **Figure 4.33**, **Figure 4.34** and **Figure 4.35**. These contour plots show the data (red dots) and the surface is only a guide to the eye scaled to the interpolated breaking time, because only few data is available. It can be seen that damage occurs earlier with higher contaminant pressure and fluence.

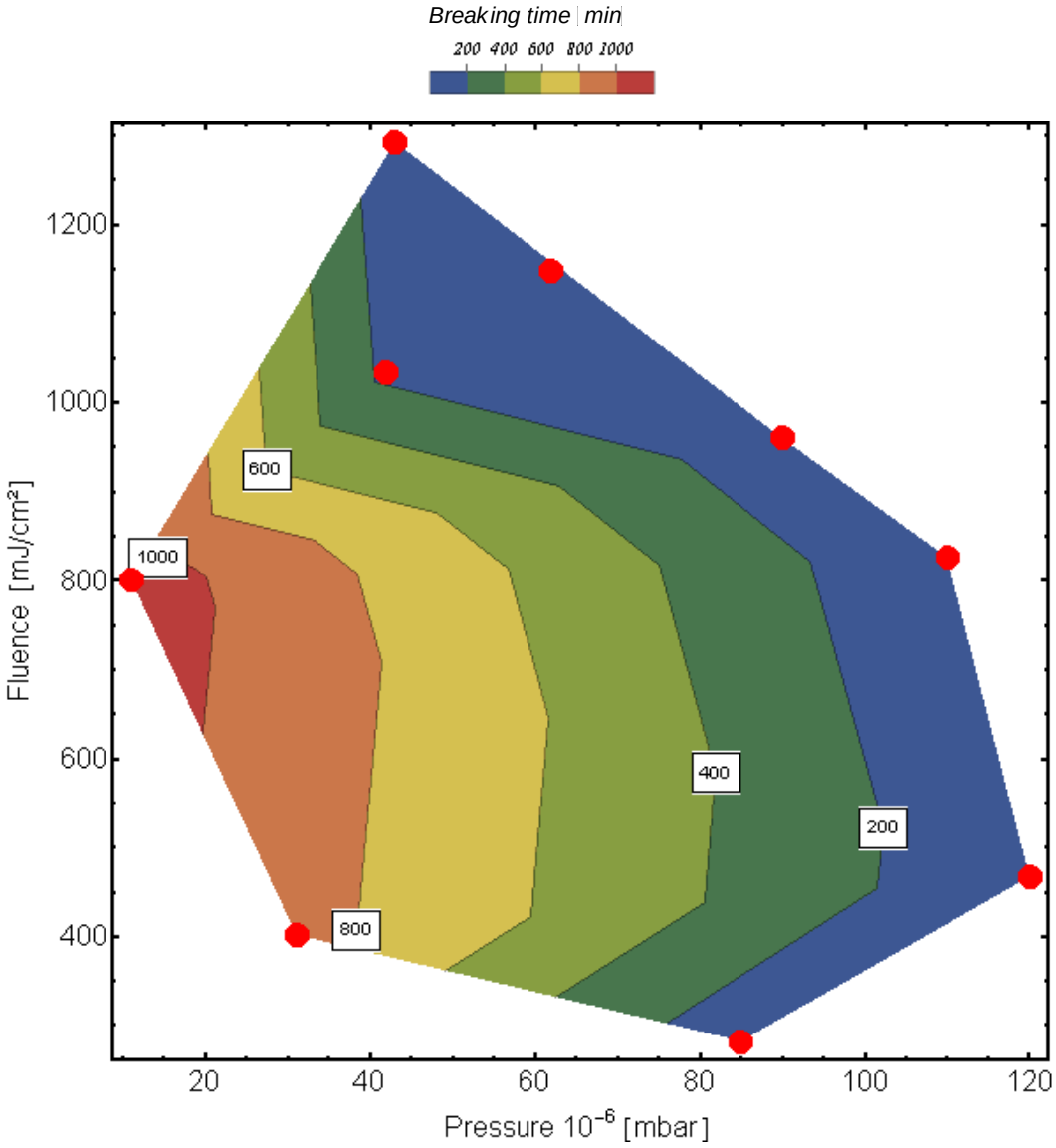

Figure 4.33: *Surface plot of the break point of EBD samples in dependence of contamination pressure and fluence.*

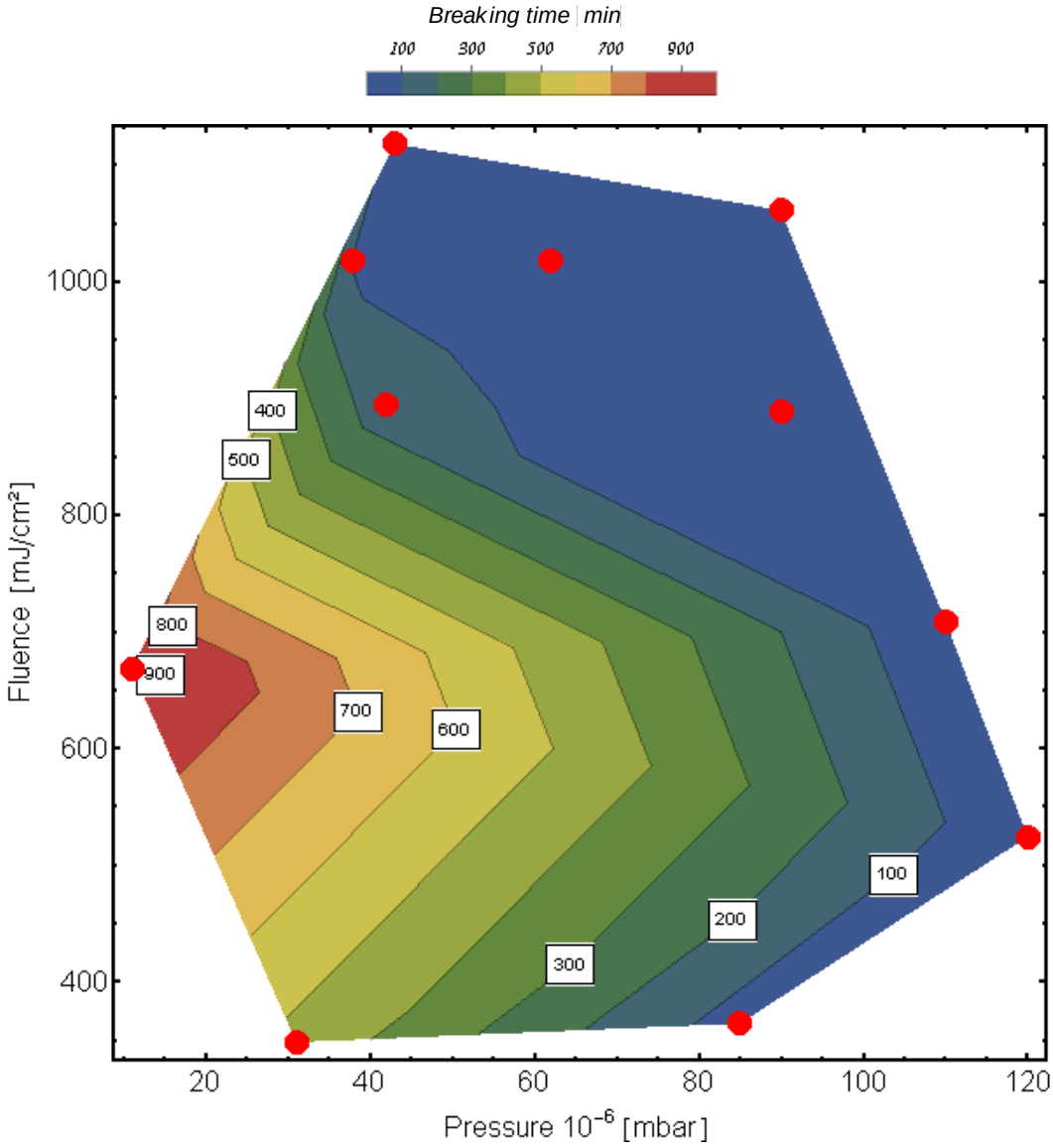

Figure 4.34: *Surface plot of the break point of MS samples in dependence of contamination pressure and fluence.*

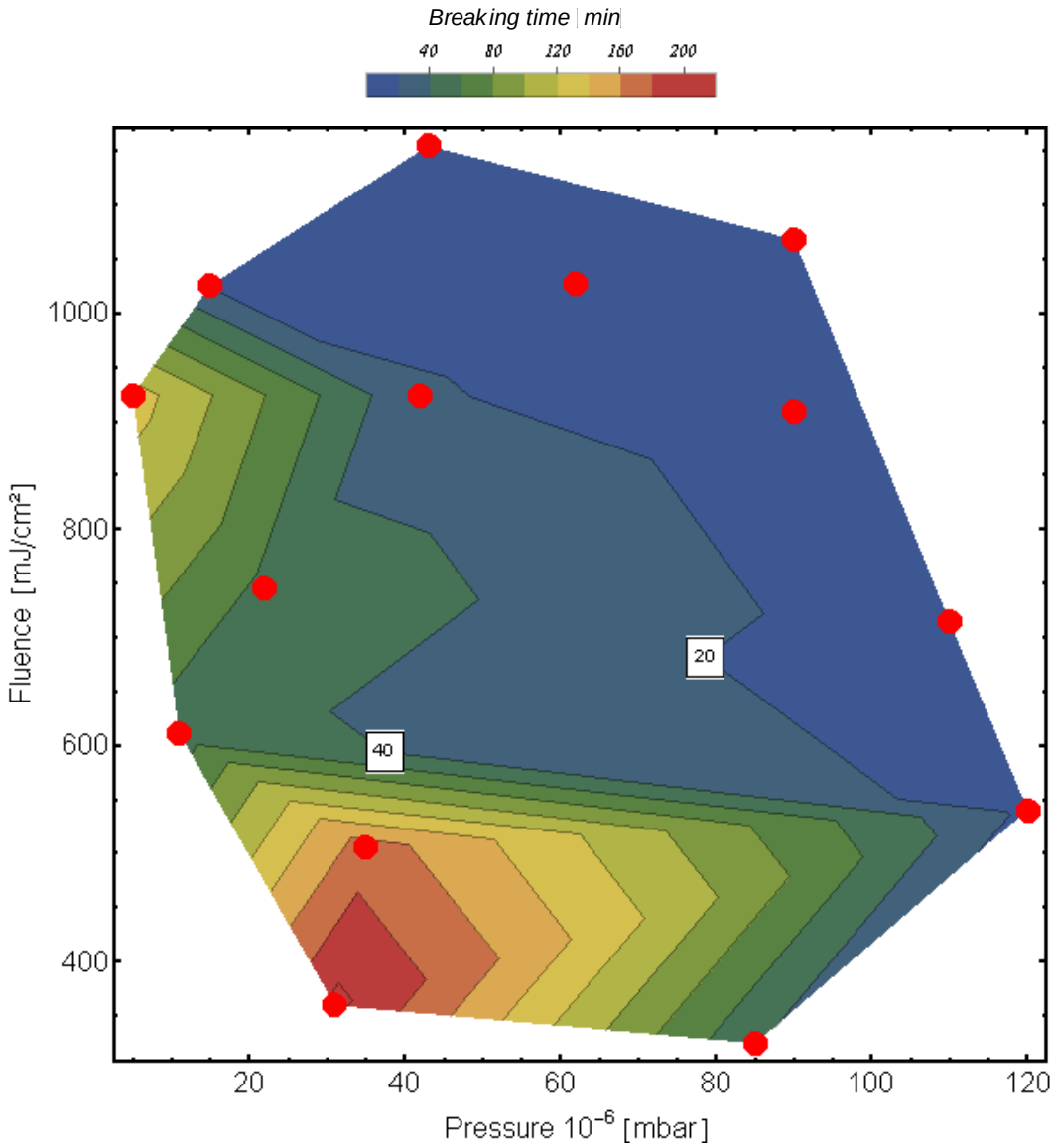

Figure 4.35: *Surface plot of the break point of IBS samples in dependence of contamination pressure and fluence.*

For direct comparison of the break point with each sample a 3D-plot shows that breakpoint of the EBD samples are always the highest. In **Figure 4.36** it can be seen that the green (EBD) surface is above the red (MS) and blue (IBS).

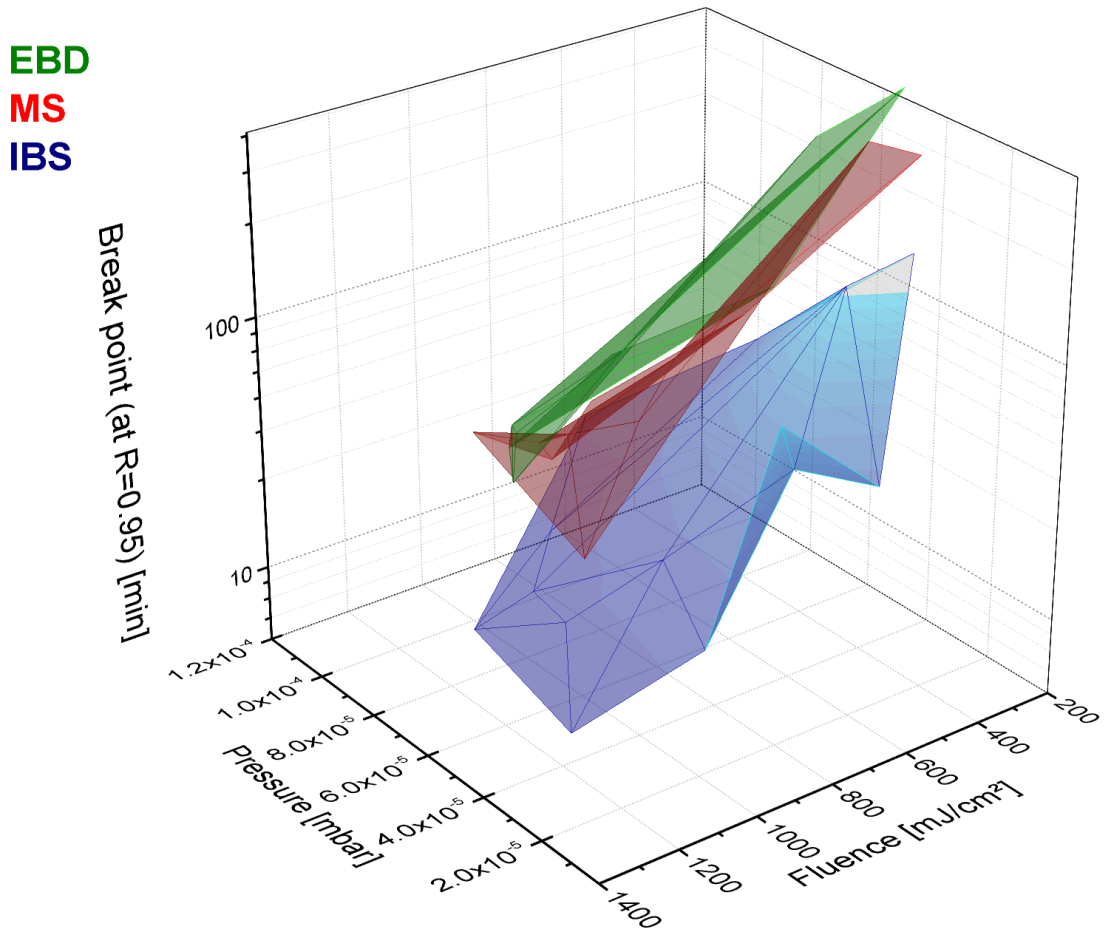

Figure 4.36: *3D-plot of the break point in dependence of fluence and contamination pressure of EBD (green), MS (red) and IBS (blue).*

CONCLUSION

LIC tests have shown that IBS coated optics show the largest damage, fastest and strongest decrease of the reflectivity than EBD and MS coated optics. MS coated optics show better results than IBS samples. But EBD samples showed best damage threshold in all LIC tests.

4.4. COMPARISON OF HR AND AR COATINGS

To HR and AR coatings comparison EBD coated samples are used and tested simultaneously. The sample holder was modified to compare a 45° HR optic with a 0° AR optic. Due to different angle of incidence on the sample the fluence needs to be corrected just for the HR sample using equation (3.2) for 0° angle of incidence peak fluence is obtained using equation (3.1).

In **Figure 4.37** EBD coated HR and AR optics are compared using reflection measurements for the HR coating and transmission measurements for the AR coating. This LIC tests were performed at different fluences for an irradiation time of 60min under a contamination pressure of 1.5×10^{-4}mbar.

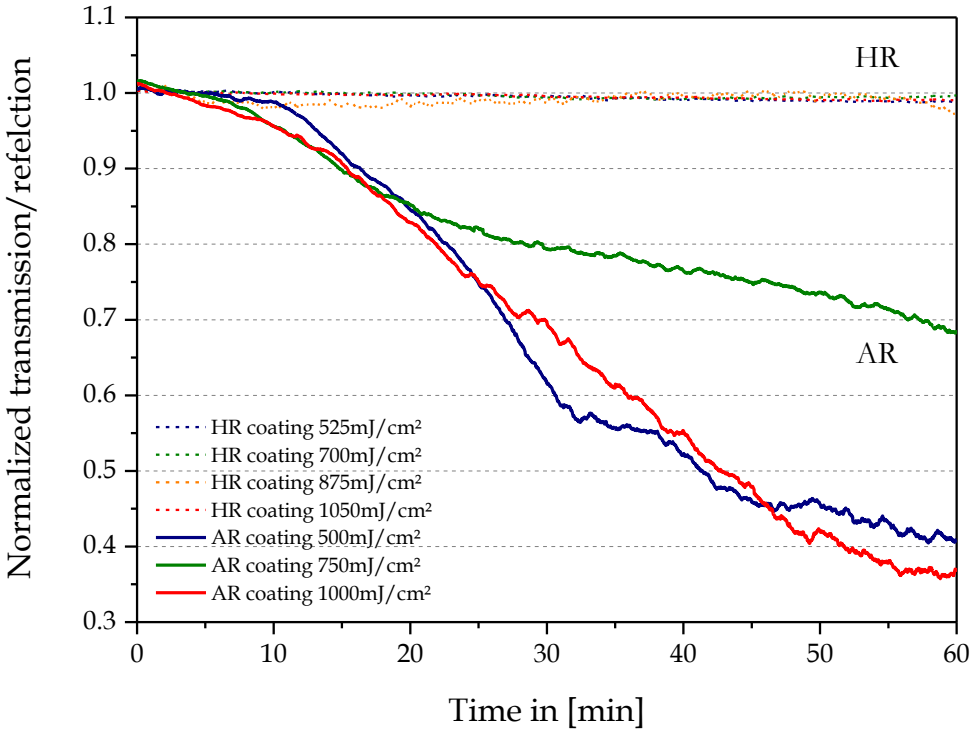

Figure 4.37: *Normalized transmission for AR sample and normalized reflection for HR sample during LIC tests with different fluence. Samples are coated in EBD process.*

It can be seen that there is only a slight loss of the transmission (2%) on HR coatings within 60min. AR coatings instead show a significant decrease in every test even under the lowest fluence (500mJ/cm²) the transmission decreased below 95% after 14min. No damage could be found with DIC microscope on HR samples of these tests. But on AR samples significant damages are visible with DIC microscope.

5. DISCUSSION

Results of the measurements will be discussed in this chapter, for contamination in section 5.1, for damage growth and behavior in section 5.2, for HR vs. AR coating comparison in section 5.3 and a finial statement gives an outlook for further research in section 5.4.

5.1. CONTAMINATION

Contamination measurements with HR coatings have shown in section 4.1 that MS samples show a lower contamination than EBD samples. But the local amount of contamination differs. MS samples show a higher local amount of contamination compared to EBD samples. IBS samples showed largest contamination and highest local amount of contamination, compare **Figure 4.3**, **Figure 4.4** and **Figure 4.5**. The local amount of contamination decreases on EBD and IBS samples at the center as a function of the irradiation time, see **Figure 4.3**, **Figure 4.4** and **Figure 4.5** (75min). The spatial intensity profiles of the laser beams are of a Gaussian density distribution, hence the fluence is higher at the center of the beam. This inhomogeneity causes the contaminant to deposit at regions of highest fluence. With further irradiation at the center of the test area the fluoresces vanishes and the deposit grows larger in time. A doughnut shaped deposit was visible on EBD and IBS samples and MS samples showed a deposit shaped that reminds of a Gaussian density distribution. Comparing FM micrographs with DIC micrographs ex-situ after damage occurred during a LIC test, exhibit that damaged areas show no fluorescence. By this it can be predicted that a decrease in the local fluorescence at the center indicates that damage is likely to occur, see **Figure 4.6**.

5.2. DAMAGE

The contamination reduces the damage threshold of the optical samples. In section 4.3 it was shown that contamination induced damage depends on the local amount of contamination, rather than the total contaminated area or the total amount of contamination. MS samples showed a higher local amount of contamination but smaller contamination area than EBD samples. This results in an earlier damage on MS than on EBD samples. Due to largest contamination area and greatest local amount of contamination on IBS samples it followed that IBS samples have the lowest damage threshold compared to MS or EBD samples. EBD samples showed the highest damage threshold. This was not expected because it has the worst material qualities of the three samples (see **Table 2.1**). In LIC tests with AR coatings using MS and EBD optics it was seen that EBD coated optics always showed an earlier decrease of transmission compared to MS coated optics [1], [16]. This shows that depending on HR or AR coatings the contamination and damage behavior changes significantly. It is expected that the rough substrate surface on IBS coated optics caused the low damage threshold on LIC tests. But additional tests will help to understand why coatings perform differently. Samples with

specifically changed coating properties like substrate roughness, thermal conductivity or absorption could be used to investigate influence of each property.

The damage morphology was investigated using an in-situ long distance microscope as described in section 4.2. With this new observation technique it was seen that MS and EBD samples show localized damages, small spots with a size of few μm which merge until they form a large damaged area. Instead, damage on IBS samples always start from the center of the beam irradiating the optical surface; this damage becomes larger in time. The damage morphology changes on EBD and MS coated optics by varying the fluence; at a lower fluence localized damages occur more pronounced on EBD and MS samples than at a higher fluence. On IBS samples the damage morphology does not change with fluence.
The damage morphology does not depending on the deposit shape because the damage morphology on MS samples is similar to EBD samples but not the shape of the contamination; compare **Figure 4.7** and **Figure 4.10**. On every LIC tested sample where damage occurred small localized damaged spots can be found with the DIC microscope. In **Figure 4.27** (right) they can be found also on IBS samples close to the edge of the damage. It seems that the damage occurs preferred on coating defects. The damaged spots are smaller in size and more concentrated on IBS samples than on EBD and MS samples.
Even EBD samples show a higher break point in time this does not necessarily mean that the damage at the end of the test (same conditions, same time) is smaller in terms of size. In **Figure 4.27** it was seen that the damage on EBD samples have a diameter of 205μm and MS of 194μm. This is due to a smaller contamination area on MS compared to EBD samples. It can be seen that the damage on IBS samples is always the largest.
By defining the break point a rough approximation of damage dynamics was done. In reflection measurements it was seen that the break point time is lower with fluence and contamination pressure. Ion Beam Sputtering samples are damaged before MS and EBD samples. Taking more data points of the break point with all three coated optics will allow better prediction of damage dynamics for future projects.

5.3. COMPARISON OF HR AND AR COATINGS

Tests comparing HR with AR coatings in chapter 4.4 have shown that HR coatings have a better damage behavior than AR coatings. The light is reflected on the HR coated surface and does not penetrate into the substrate. Those tests were performed only for EBD coated optics. For future investigation of further LIC tests other coating processes in HR and AR comparison are of interest. This will help to understand the influences of contamination process better.

5.4. OUTLOOK

This results show that HR coatings should be made by different coating processes other than AR coatings to avoid laser-induced contamination. For space-based laser systems this does not necessarily mean that the EBD coated optics are a solution because in this LIC tests the contamination process was enforced. In real space-based laser systems contaminant

concentration will be lower and EBD coated optics show vacuum effect therefore they are not suitable for space applications. Most practical solution is to run the laser system under artificial oxygen atmosphere using MS coated HR optics because former test have shown that oxygen avoids the organic deposit formation [1], [5].

It is still not completely understood what drives the contamination process between organic molecules and laser beam. One possible effect which might cause this interaction is the optical tweezers effect. This is the force on a dipole in an electromagnetic field. The dipole is cause by high energy laser pulses on the contaminant and the force applied to this dipole is proportional to the gradient of the intensity profile of the laser beam. Under high vacuum this force makes small molecules moving until they reach an optical surface where the contaminant deposits. To investigate the influence of the optical tweezers effect on the LIC process, a test procedure irradiating the samples with an interference pattern of two beams can be developed. The interference pattern shows a higher gradient of the intensity profile than the Gaussian beam profile. The beam line of presented LIC test bench allows an adjustment to create an interference pattern on one sample which will be detectable under FM.
A possibility to examine damage behavior in-situ, is to detect the diffraction pattern after beam passes UHV chamber. The analysis of the diffraction pattern allows detecting small defects on the optical sample.
Fourier Transform IR absorption spectroscopy of the deposit on the samples can be used in future work to understand chemical process during deposit formation.

This knowledge will allow increasing the laser energy in future space-based laser systems. This allows long term space missions with more precise measurements like wind speed measurements in future.

6. APPENDIX

6.1. RELATED PUBLICATIONS

1) *H. Schröder; P. Wagner; D. Kokkinos; W. Riede and A. Tighe* - **"Laser-induced contamination and its impact on laser damage threshold"**, Proc. SPIE 8885, Laser-Induced Damage in Optical Materials: 2013, 88850R (November 14, 2013)

6.2. LIST OF PERFORMED LIC TESTS

Test #	Internal EBD sample #	Internal MS sample #	Internal IBS sample #	Contaminant pressure x10^{-4} [mbar] ±10%	Fluence (45°) [mJ/cm²] ±10%	Duration [min]	Purpose, Annotation
1	1193	1103	1233	4	500	60	Damage threshold
2	1193	1103	1233	1.2	750	65	Damage threshold
3	1193	1103	1233	1.4	1000	60	Damage threshold
4	1193	1103	1233	1.4	1000	60	Damage threshold
5	1193	1103	1233	0.85	300	60	Damage threshold
6	1193	1103	1233	1.2	500	76	Damage threshold
7	1193	1103	1233	1.1	750	60	Damage threshold
8	1193	1103	1233	0.9	800	60	Damage threshold
9	1193	1103	1233	0.9	1000	60	Damage threshold
10	1194, 1213	-	-	0.5	350	60	Comparison HR vs. AR
11	1194, 1213	-	-	0.4	500	60	Comparison HR vs. AR
12	1194, 1213	-	-	0.5	700	60	Comparison HR vs. AR
13	1194, 1213	-	-	0.5	850	60	Comparison HR vs. AR
14	1194, 1213	-	-	0.5	1050	60	Comparison HR vs. AR
15	1195	1107	1234	0.5	300	15	Fluorescence
16	1195	1107	1234	0.4	300	20	Fluorescence
17	1195	1107	1234	0.4	300	25	Fluorescence
18	1195	1107	1234	0.45	300	30	Fluorescence
19	1195	1107	1234	0.45	300	35	Fluorescence
20	1195	1107	1234	0.45	300	40	Fluorescence
21	1195	1107	1234	0.48	300	45	Fluorescence
22	1195	1107	1234	0.48	300	50	Fluorescence

23	1195	1107	1234	0.48	300	55	Fluorescence
24	1195	1107	1234	0.48	300	60	Fluorescence
25	1195	1107	1234	0.48	300	52	Fluorescence
26	1195	1107	1234	0.48	300	65	Fluorescence
27	1195	1107	1234	0.48	300	72	Fluorescence
28	1195	1107	1234	0.48	300	75	Fluorescence
29	1195	1107	1234	0.48	300	80	Fluorescence
30	1195	1107	1234	0.48	300	85	Fluorescence
31	1195	1107	1234	0.48	300	90	Fluorescence
32	1195	1107	1234	0.48	300	95	Fluorescence
33	1195	1107	1234	0.48	300	105	Fluorescence
34	1195	1107	1234	0.48	300	120	Fluorescence
35	1196	1108	1235	0.5	1000	150	Long distance microscope
36	1196	1108	1235	0.15	1000	180	Long distance microscope
37	1196	1108	1235	0.35	500	210	Long distance microscope
38	1196	1108	1235	0.35	750	120	Long distance microscope
39	1196	1108	1235	0.6	1050	60	Long distance microscope
40	1196	1108	1235	0.4	1050	60	Long distance microscope
41	1196	1108	1235	0.4	1000	60	Long distance microscope
42	1196	1108	1235	0.4	1000	60	Long distance microscope
43	1196	1108	1235	0.4	1200	60	Long distance microscope
44	1196	1108	1235	0.3	350	1740	Long distance microscope
45	1196	1108	1235	0.34	450	1440	Long distance microscope
46	1196	1108	1235	0.35	450	1440	Long distance microscope
47	1196	1108	1235	0.35	700	1440	Long distance microscope
48	1196	1108	1235	0.35	700	1440	Long distance microscope
49	1196	1108	1235	0.6	700	360	Long distance microscope
50	1196	1108	1235	0.32	700	360	Long distance microscope
51	1196	1108	1235	0.35	700	360	Long distance microscope

7. REFERENCES

[1] **Optical components materials and process development and validation for high power space borne lasers** Phase I Report - *H. Schröder, G. Batavičiūtė* , DLR, *Istvan Balasa*, Laser Zentrum Hannover e.V. (2013)

[2] *S. Becker, A. Pereira, P. Bouchut, F. Geffraye, and C. Anglade*, "**Laser-induced contamination of silica coatings in vacuum**" - SPIE Vol. 6403, 64030I, (2007).

[3] **ADM-Aeolus Science Report** - ESA (2008)

[4] **Optik für Ingenieure** Grundlagen, 3. Aufl. – *F. Pedrotti, L. Peddrotti, W. Bausch, H. Schmidt,* Springer (2005)

[5] *Adrian P. Tighe; Federico Pettazzi; Jorge Alves; Denny Wernham; W. Riede, et al.* - **"Growth mechanisms for laser induced contamination on space optics in vacuum"**, Proc. SPIE 7132, Laser-Induced Damage in Optical Materials: 2008, 71321L (December 30, 2008)

[6] *Michael Huff*, (2002) **"MEMS fabrication"**, Sensor Review, Vol. 22 Iss: 1, pp.18 – 33

[7] *Holger Blaschke*, **Charakterisierung Optischer Schichten**, Laser Zentrum Hannover e.V. (2010)

[8] **Laser damage risks and mitigation for the ALADIN instrument on ADM-Aeolus** - *TEC-Support Team,* ESA (2005, AE-TN-ESA-AL-0008)

[9] **Handbook of ion sources** - *Bernhard Wolf* , CRC Press (1995), p. 222.

[10] *M. Mende, L. Jensen, H. Ehlers, W. Riggers, H. Blaschke, D. Ristau*, **"Laser induced damage of pure and mixture material high reflectors for 355nm and 1064nm wavelength"**, Advances in Optical Thin Films IV, Proc. of SPIE 8168-21 (2011).

[11] **Coating methods for high precision laser optics with special focus on Ion Beam Sputtering** - *Michael Kennedy,* Laser 2011 Munich, Talk (2011)

[12] **Advantages of Ion-Beam-Sputtered (IBS) Dielectric Thin Films**, http://www.precisionphotonics.com/individual_technology_tp.asp?id=6, Precision Photonics (10.01.2014)

[13] **Ion Beam Sputtering: Practical Applications to Electron Microscopy**, Applications Laboratory Report 91 - South Bay Inc. (2014)

[14] **Differential interference contrast microscopy** - Wikipedia, http://en.wikipedia.org/wiki/File:DIC_Light_Path.png

[15] **Anatomy of the Fluorescence Microscope** – Olympus, http://www.olympusmicro.com/primer/techniques/fluorescence/anatomy/fluoromicroanatomy.html

[16] *H. Schröder; P. Wagner; D. Kokkinos; W. Riede and A. Tighe* - **"Laser-induced contamination and its impact on laser damage threshold"**, Proc. SPIE 8885, Laser-Induced Damage in Optical Materials: 2013, 88850R (November 14, 2013)

[17] *Martin und Johannes Ebert*, „**Magnetron-Sputtern im Mikrowellenplasma im Vergleich zu konventionellen Aufdampfverfahren“** – Photonik 032 (1/2002)

[18] *P.J. Kelly, R.D. Arnell*, "**Magnetron sputtering: a review of recent developments and applications**" - Vacuum 56 (2000) 159.

[19] **DIN EN ISO 11145** (2006) - Optik und Photonik/Laser und Laseranlagen/Begriffe und Formelzeichen